Interaction of Binuclear Transition Metal Complexes with DNA

Edward A. Kesicki, Mark A. DeRosch, Laurie H. Freeman, Christine L. Walton, Daniel F. Harvey,* and William C. Trogler*

Department of Chemistry-0358, University of California at San Diego, 9500 Gilman Drive, La Jolla, California 92093-0358

*Received May 11, 1993**

A series of binucleating tetrakis(methylimidazole) ligands of the general type $(MeIm)_2C(OH)$–spacer–$C(OH)(MeIm)_2$ were prepared, where MeIm = 1-methylimidazol-2-yl and the spacer was one of several different rigid (**5** = 1,4-C_6H_4, **6** = *trans*-C_2H_2, **14** = (2α,3aβ,5α,6aβ)-octahydro-3a,6a-dimethylpentalene, **15** = (2α,3aα,5α,6aα)-octahydro-3a,6a-dimethylpentalene, **16** = 2α,3aα,5β,6aα)-octahydro-3a,6a-dimethylpentalene) or flexible ($(CH_2)_n$, **7**, n = 0; **8**, n = 1; **9**, n = 2; **10**, n = 3; **11**, n = 8) spacers. A highly rigid binucleating ligand, (3aα,6aα)-octahydro-2,5-bis(bis(1-methylimidazol-2-yl)methylene)-3a,6a-dimethylpentalene (**17**), was also prepared and characterized. The effectiveness of the rigid binuclear complexes of Cu(II), Ni(II), and Zn(II) as catalysts for the hydrolysis of the phosphate diester sodium bis(4-nitrophenyl) phosphate was similar to corresponding mononuclear complexes with ligand **4** = $(MeIm)_2C(OH)CH_3$ or bipyridine. A significant DNA binding ability was observed for the binuclear complexes, which was not evident with the mononuclear compounds. In gel electrophoresis mobility studies, the cationic dimetal complexes with the tetrakis(methylimidazole) ligands significantly retarded the migration of supercoiled plasmid DNA. The binucleating ligands with flexible organic spacer groups and the mononuclear metal complexes did not show this effect. In ultrafiltration experiments with tritium labeled ligands, all the cationic dimetal complexes showed evidence for DNA binding, whereas the mononuclear complexes of **4** did not. Similar results were obtained for DNA precipitation studies. Without added metal ions, none of the ligands evidenced a significant DNA binding ability. Simple amine polycations and mononuclear cations, such as Mg(II), were not able to disrupt the binding of the binuclear complexes to DNA, unless added in a large excess. Nickel(II) complexes that contained ligands **7**, **9**, and **15** were crystallized and characterized by X-ray crystallography. In addition, the Zn(II) complexes present in solution with ligands **4**, **14**, and **15** were studied by ^1H NMR spectroscopy. Reasons for the enhanced binding ability of dimetal complexes to DNA and the role of a flexible or rigid spacer group are discussed.

Introduction

In both biological and abiological systems, metal ions and metal complexes may interact with DNA by several modes. Cations, such as Na^+, K^+, and Mg^{2+}, act as counterions to formally neutralize the polyanionic charge of the phosphodiester backbone of DNA.[1] In cationic coordination complexes, such as $Ru(phen)_3^{2+}$, ligands associated with the metal have been suggested to be capable of selective interactions with specific conformations of the DNA double helix[2] or with specific DNA base sequences.[3] The anti-tumor agent Cisplatin binds mainly to the N7 residues of guanine in the major groove of B-DNA.[4] A variety of metal complexes have also been shown to increase the rate of phosphate ester hydrolysis.[5] Through interactions with proteins, metal ions participate in both DNA recognition[6] and phosphodiester hydrolysis.[7] Redox properties of a variety of metals have been exploited as DNA cleaving agents.[8] The anticancer drug bleomycin relies on a metal redox center for its DNA cleaving reaction.[9]

* Abstract published in *Advance ACS Abstracts*, October 15, 1993.

(1) (a) Eichhorn, G. L.; Shin, Y. A. *J. Am. Chem. Soc.* **1968**, *90*, 7323–7328. (b) Marzilli, L. G. *Prog. Inorg. Chem.* **1977**, *23*, 255–378. (c) Barton, J. K.; Lippard, S. J. *Met. Ions Biol.* **1980**, *1*, 31–113.

(2) (a) For a recent review, see: Pyle, A. M.; Barton, J. K. In *Progress in Inorganic Chemistry: Bioinorganic Chemistry*; Lippard, S. J., Ed.; Wiley: New York, 1990, Vol. 38, pp 413–475. (b) Barton, J. K. *Science* **1986**, *233*, 727–734. (c) Hiort, C.; Norden, b.; Rodger, A. *J. Am. Chem. Soc.* **1990**, *112*, 1971–1982. (d) Eriksson, M.; Leijon, M.; Hiort, C.; Norden, B.; Graslund, A. *J. Am. Chem. Soc.* **1992**, *114*, 4933–4934. (e) Fleisher, M. B.; Mei, H.-Y.; Barton, J. K. In *Nucleic Acids and Molecular Biology*; Eckstein, F., Lilley, D. M. J., Eds.; Springer-Verlag: Berlin, 1988; Vol. 2, pp 65–84. (f) Chen, X.; Burrows, C. J.; Rokita, S. E. *J. Am. Chem. Soc.* **1992**, *114*, 322–325.

(3) (a) Ward, B.; Skorobogaty, A.; Dabrowiak, J. C. *Biochemistry* **1986**, *25*, 6875–6883. (b) Van Atta, R. B.; Bernadou, J.; Meunier, B.; Hecht, S. M. *Biochemistry* **1990**, *29*, 4783–4789. (c) Lippard, S. J. *Acc. Chem. Res.* **1978**, *11*, 211–217. (d) Barton, J. K. *Comments Inorg. Chem.* **1985**, *3*, 321–348.

(4) (a) Sherman, S. E.; Lippard, S. J. *Chem. Rev.* **1987**, *87*, 1153–1181. (b) Coll, M.; Sherman, S. E.; Gibson, D.; Lippard, S. J.; Wang, A. H. *Biomol. Struct. Dyn.* **1990**, *8*, 315–330.

(5) (a) For a recent review, see: Hendry, P.; Sargeson, A. M. In *Progress in Inorganic Chemistry: Bioinorganic Chemistry*; Lippard, S. J., Ed.; Wiley: New York, 1990, Vol. 38, pp 201–258. (b) Basile, L. A.; Raphael, A. L.; Barton, J. K. *J. Am. Chem. Soc.* **1987**, *109*, 7550–7551. (c) Hendry, P.; Sargeson, A. M. *J. Am. Chem. Soc.* **1989**, *111*, 2521–2527. (d) Chin, J.; Banaszczyk, M. *J. Am. Chem. Soc.* **1989**, *111*, 4103–4105. (e) Gellman, S. H.; Petter, R.; Breslow, R. *J. Am. Chem. Soc.* **1986**, *108*, 2388–2394. (f) Milburn, R. M.; Gautam-Basak, M.; Tribolet, R.; Sigel, H. *J. Am. Chem. Soc.* **1985**, *107*, 3315–3321. (g) Sigel, H.; Hoffstetter, F.; Martin, R. B.; Milburn, R. M.; Scheller-Krattiger, V.; Scheller, K. H. *J. Am. Chem. Soc.* **1984**, *106*, 2521–2527. (h) Chin, J. *Acc. Chem. Res.* **1991**, *24*, 145–152. (i) Morrow, J. R.; Trogler, W. C. *Inorg. Chem.* **1988**, *27*, 3387–3394. (j) Morrow, J. R.; Trogler, W. C. *Inorg. Chem.* **1989**, *28*, 2330–2333. (k) DeRosch, M. A.; Trogler, W. C. *Inorg. Chem.* **1990**, *29*, 2409–2416.

(6) (a) O'Halloran, T. V. *Met. Ions Biol. Syst.* **1989**, *25*, 105–146. (b) Berg, J. M. *Met. Ions Biol. Syst.* **1989**, *25*, 235–254. (c) Pavletich, N. P.; Pabo, C. O. *Science* **1991**, *252*, 809–817. (d) Pan, T.; Coleman, J. E. *Proc. Natl. Acad. Sci. U.S.A.* **1989**, *86*, 3145–3149. (e) Wu, F. Y.-H.; Wu, C.-W. *Met. Ions Biol. Syst.* **1983**, *15*, 157–192.

(7) (a) Cotton, F. A.; Hazen, E. E. Jr.; Legg, M. J. *Proc. Natl. Acad. Sci. U.S.A.* **1979**, *76*, 2551–2555. (b) Anfinsen, C. B.; Cuatrecasas, P.; Taniuchi, H. In *The Enzymes*; Boyer, P. D., Ed.; Academic Press, Inc.: New York, 1971; Vol. IV, pp 177–204. (c) Frederick, C. A.; Grable, J.; Melia, M.; Samudzi, C.; Jen-Jacobson, L.; Wang, B.-C.; Greene, P.; Boyer, H. W.; Rosenberg, J. M. *Nature* **1984**, *309*, 327–331. (d) Brown, R. S.; Dewan, J. C.; Klug, A. *Biochemistry* **1985**, *24*, 4785–4801.

(8) (a) Tullius, T. D. In *Nucleic Acids and Molecular Biology*; Eckstein, F., Lilley, D. M. J., Eds.; Springer-Verlag: Berlin, 1989; Vol. 3, pp 1–12. (b) Sigman, D. S.; Spassky, A. In *Nucleic Acids and Molecular Biology*, Eckstein, F., Lilley, D. M. J., Eds.; Springer-Verlag: Berlin, 1989; Vol. 3, pp. 13–27. (c) Sigman, D. S. *Acc. Chem. Res.* **1986**, *19*, 180–186. (d) Chen, X.; Rokita, S. E.; Burrows, C. J. *J. Am. Chem. Soc.* **1991**, *113*, 5884–5886. (e) Groves, J. T.; Farrell, T. P. *J. Am. Chem. Soc.* **1989**, *111*, 4998–5000. (f) Stubbe, J. *Chem. Rev.* **1987**, *87*, 1107–1136. (g) Basile, L. A.; Barton, J. K. *J. Am. Chem. Soc.* **1987**, *109*, 7548–7550. (h) Youngquist, R. S.; Dervan, P. B. *J. Am. Chem. Soc.* **1987**, *109*, 7654–7566. (i) Dervan, P. B. *Methods Enzymol.* **1991**, *208*, 497–515. (j) Dixon, W. J.; Hayes, J. J.; Levin, J. R.; Weidner, M. F.; Dombroski, B. A.; Tullius, T. D. *Methods Enzymol.* **1991**, *208*, 380–413.

0020-1669/93/1332-5851$04.00/0

As part of a project directed toward the development of phosphodiester hydrolysis catalysts,[5i-k] we were interested in determining whether bimetallic systems of the general formula **1** were capable of accomplishing the process outlined in eq 1.

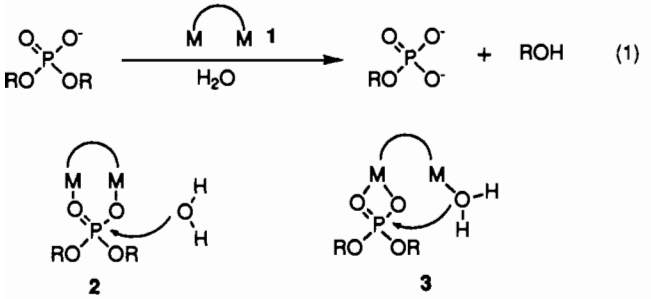

Among the many possibilities, this reaction could be envisioned as occurring either through intermediate **2**, where the phosphodiester bridges the two metals, or through intermediate **3**, where one metal binds to the phosphodiester in a bidentate fashion, while the other metal directs a hydroxo or aquo ligand to the activated phosphorous center. Bimetallic sites that might serve as biological equivalents of these two modes of hydrolysis have been found in several hydrolase enzymes,[10] as well as in DNA polymerase I.[11]

Our initial goal was to design ligands that would hold two metals at an appropriate distance for phosphodiester binding and hydrolysis through one of these pathways. Studies with simple phosphodiesters demonstrated that hydrolysis occurred only at a slightly accelerated rate in the presence of several of these metal–ligand complexes. Studies performed with DNA showed no hydrolytic activity. Instead, in several cases, very strong binding of the ligand:dimetal complexes to the DNA was encountered, whereas related mononuclear complexes evidenced little binding.

Though the interactions of monometallic complexes with DNA have been investigated extensively, bimetallic complexes, wherein both metals are available for interaction with the DNA framework, have been seldom examined.[12] Both bis-intercalating agents[13] and intercalator/metal conjugates[14] exhibit enhanced DNA binding ability in comparison to monofunctional agents. Bimetallic complexes, having both metals available for coordination to the DNA, may bind much more tightly than 2 equiv of a corresponding monometallic complex through cooperativity from two-point binding to DNA.[15] This paper describes the interaction of several bimetallic complexes with DNA in comparison with their mononuclear analogues. These studies demonstrate that the DNA binding ability of these binuclear complexes depends on the conformation and flexibility of the spacer unit between the two metal coordination sites.

Experimental Section

General Procedures. Melting points are uncorrected and were obtained using a Mel-Temp II melting point apparatus. All reagents were purchased from commercial sources and used without purification, except as noted below. Tetrahydrofuran (THF) was purified by distillation from potassium/benzophenone ketyl under a dinitrogen atmosphere. 1-Methylimidazole was distilled at reduced pressure and stored over molecular sieves (3 Å). HPLC grade water (Fisher) or glass distilled water was used for the preparation of aqueous solutions. ^{1}H NMR experiments were performed at 300 MHz with a G.E. QE-300 spectrometer, or at 500 MHz with a Varian Unity 500 spectrometer, as specified below. Low-temperature NMR experiments were conducted by cooling the sample to −80 °C and allowing the sample to equilibrate for 15 min after the probe had reached the desired temperature. The titrations with metal solutions were performed by adding aliquots of a 1.0 M solution of $Zn(NO_3)_2{\cdot}6H_2O$ in MeOH-d_4 and allowing the sample to reequilibrate for 5 min. Gel electrophoresis experiments were conducted on 1% agarose (Fisher Scientific, high-melting DNA grade) in a home-built 10 cm horizontal minigel apparatus at 60–75 V until the bands were adequately separated (45–90 min) with the use of a Hewlett-Packard Model 712B power supply. Ethidium bromide (Sigma) was used as a DNA stain.[16] The fluorescent ethidium–DNA bands were viewed on a Haake-Büchler transilluminator and photographed with a Photodyne camera (red filter using Polaroid 667 film).

X-ray Crystal Structure Determinations. X-ray data were collected with the use of a Nicolet R3m/V automated diffractometer equipped with a Mo X-ray tube and a graphite crystal monochromator. The orientation matrix and unit cell parameters were determined from 25 machine centered reflections with $15 < 2\theta < 30°$. Intensities of three check reflections were monitored after every 100 or 200 reflections during data collection, as specified in the text. No absorption correction was applied. All calculations were performed on a MicroVAX II computer with the use of the SHELXTL PLUS program package. Protons were fixed in idealized positions with isotropic parameters. Crystal data, data collection, and refinement parameters are summarized in Table I.

Tritiation of 1,1-Bis(1-methylimidazol-2-yl)-1-hydroxyethane (4). To a suspension of **4**[17] (41.0 mg, 0.20 mmol) in THF (3 mL) at −78 °C was added *tert*-butyllithium (1.7 M in pentane, 1.4 mL, 2.45 mmol). After being warmed to room temperature, the reaction mixture was stirred until the solution became clear (approximately 5–10 min). Tritiated water (1 Ci/g, 0.115 mL, 6.5 mmol) was then added and the reaction mixture was stirred for 15 min at room temperature. The mixture was diluted with aqueous K_2CO_3 solution (5% w/v, 5 mL) and extracted with chloroform (6 × 6 mL). The combined organics were washed with water (3 × 3 mL) and dried over K_2CO_3. Solvent was evaporated under a stream of nitrogen, and the resulting solid was recrystallized by dissolving in chloroform and layering with hexanes to give white crystals of [^{3}H]-**4** (13.7 mg, 33% yield, 10.8 Ci/mol, 60% exchange). ^{1}H NMR data matched that of **4**.

1,4-Bis(bis(1-methylimidazol-2-yl)hydroxymethyl)benzene (5). To a stirred solution of 1-methylimidazole (3.91 mL, 48.88 mmol) in THF (80 mL) at −78 °C was added *n*-butyllithium (32.6 mL, 48.88 mmol, 1.6 M in hexane) over a 10 min period. After 30 min of stirring at −78 °C, dimethyl terephthalate (1.19 g, 6.11 mmol) in THF (20 mL) was added dropwise over a 30 min period. The reaction mixture was then warmed to room temperature and stirred for 6 h. After addition of water and extraction with EtOAc (4 × 100 mL), the combined organics were dried over Na_2CO_3 and concentrated in vacuo. The resultant light yellow solid was purified by chromatography on silica gel to give tetraimidazole **5** (1.51 g, 54% yield). Mp: 242.5–243 °C. ^{1}H NMR (300 MHz, CD_3OD:D_2O {50:50}): δ 7.19 (s, 4 H), 7.11 (br s, 4 H), 6.84 (d, J = 1.0 Hz,

(9) Stubbe, J.; Kozarich, J. W. *Chem. Rev.* **1987**, *87*, 1107–1136.
(10) (a) Kim, E. E.; Wyckoff, H. W. *J. Mol. Biol.* **1991**, *218*, 449–464. (b) Dietrich, M.; Münstermann, D.; Suerbaum, H.; Witzel, H. *Eur. J. Biochem.* **1991**, *199*, 105–113.
(11) Beese, L. S.; Steitz, T. A. *EMBO J.* **1991**, *10*, 25–33.
(12) (a) Jones, D. R.; Lindoy, L. F.; Sargeson, A. M. *J. Am. Chem. Soc.* **1984**, *106*, 7807–7819. (b) Breslow, R.; Singh, S. *Bioorg. Chem.* **1988**, *16*, 408–417. (c) Chung, Y.; Akkaya, E. U.; Venkatachalam, T. K.; Czarnik, A. W. *Tetrahedron Lett.* **1990**, *31*, 5413–5416. (d) Qu, Y.; Farrell, N. *J. Am. Chem. Soc.* **1991**, *113*, 4851–4857 and references cited therein.
(13) (a) Ikeda, R. A.; Dervan, P. B. *J. Am. Chem. Soc.* **1982**, *104*, 296–297. (b) Gaugain, B.; Barbet, J.; Oberlin, R.; Roques, B. P.; Le Pecq, J.-B. *Biochemistry*, **1978**, *17*, 5071–5078. (c) Hansen, J. B.; Koch, T.; Buchardt, O.; Nielsen, P. E.; Norden, B.; Wirth, M. *J. Chem. Soc., Chem. Commun.* **1984**, 509–511. (d) Hansen, J. B.; Koch, T.; Buchardt, O.; Nielsen, P. E.; Wirth, M.; Norden, B. *Biochemistry*, **1983**, *22*, 4878–4886. (e) Helbecque, N.; Bernier, J.-L; Henichart, J.-P. *Biochem. J.* **1985**, *225*, 829–832.
(14) Bowler, B. E.; Ahmed, K. J.; Sundquist, W. I.; Hollis, L. S.; Whang, E. E.; Lippard, S. J. *J. Am. Chem. Soc.* **1989**, *111*, 1299–1306.
(15) For general discussions see: (a) Cotton, F. A.; Wilkinson, G. *Advanced Inorganic Chemistry*, 5th ed., Wiley: New York; 1988; pp 45–47. (b) Jencks, W. P. *Catalysis in Chemistry and Enzymology*, 1987; pp 372–374. (c) Fraústo da Silva, J. J. R. *J. Chem. Ed.* **1983**, *60*, 390–392. (d) Rosseinsky, D. R. *J. Chem. Soc., Dalton Trans.* **1979**, 731–734. (e) Myers, R. T. *Inorg. Chem.* **1978**, *17*, 952–958. (f) Bell, C. F. *Principles and Applications of Metal Chelation*; Clarendon Press: Oxford, England 1977.
(16) Maniatis, T.; Fritsch, E. F.; Sambrock, J. *Molecular Cloning*; Cold Spring Harbor Laboratory: Cold Spring Harbor, NY, 1982.
(17) (a) Byers, P. K.; Canty, A. J. *Organometallics* **1990**, *9*, 210–220. (b) Harvey, D. F.; Christmas, C. A.; McCusker, J. A.; Hagen, P. A.; Chadha, R. K.; Hendrickson, D. A. *Angew. Chem., Int. Ed. Engl.* **1991**, *30*, 598–600. (c) McCusker, J. K.; Christmas, C. A.; Hagen, P. M.; Chadha, R. K.; Harvey, D. F.; Hendrickson, D. N. *J. Am. Chem. Soc.* **1991**, *113*, 6114–6124.

Table I. Crystal, Data Collection, and Refinement Parameters for $[Ni_2(\mathbf{15})_2Cl]Cl_3 \cdot 8H_2O$ (**18**), $[Ni_2(\mathbf{9})_2(NO_3)(H_2O)_2](NO_3)_3 \cdot 2H_2O$ (**19**), and $[Ni_2(\mathbf{7})_2(NO_3)(H_2O)_2](NO_3)_3 \cdot 3H_2O$ (**20**)

	18	**19**	**20**
		Crystal Data	
formula	$C_{56}H_{76}Cl_4N_{16}Ni_2O_{12}$	$C_{44}H_{68}N_{20}Ni_2O_{20}$	$C_{40}H_{62}N_{20}Ni_2O_{21}$
color; habit	blue; rhombs	purple; rhombs	purple; rhombs
crystal size, mm	0.3 × 0.4 × 0.4	0.2 × 0.4 × 0.6	0.3 × 0.3 × 0.1
cryst syst	monoclinic	monoclinic	monoclinic
space group	$P2_1/n$	$P2_1$	$P2_1/n$
unit cell dimens			
a, Å	14.087(4)	13.846(6)	18.676(4)
b, Å	22.924(9)	14.311(6)	13.438(3)
c, Å	22.087(6)	16.832(2)	21.643(6)
β, deg	95.46(2)	93.61(3)	100.70(2)
volume, Å^3	7100(4)	3328(2)	5337(2)
Z	4	2	4
fw	1424.5	1314.6	1262.4
D(calcd), g/cm^3	1.333	1.312	1.571
abs coeff, mm^{-1}	0.747	0.643	0.799
F(000)	2976	1376	2616
		Data Collection	
diffractometer used	Nicolet R3m/V	Nicolet R3m/V	Nicolet R3m/V
radiation	MoKα (λ = 0.71073 Å)	MoKα (λ = 0.71073 Å)	MoKα (λ = 0.71073 Å)
temp, K	294	298	298
monochromator		highly oriented graphite crystal	
2θ range, deg	3.0–45.0	4.0–45.0	4.0–45.0
scan type	ω	2θ	Wyckoff
scan speed (°/min in ω)	variable, 2.00–15.00	variable, 3.50–15.00	variable, 3.50–15.00
scan range (ω), deg	2.00	1.10 plus Kα separation	1.00
std reflcns	3 every 200 reflcns	3 every 100 reflcns	3 every 197 reflcns
no. of reflcns collcd	11277	6422	8640
no. of indept reflcns	9257 (R_{int} = 9.63%)	6414 (R_{int} = 5.93%)	6989 (R_{int} = 4.74%)
no. of obsd reflcns	4957 ($F > 6.0\sigma(F_o)$)	2797 ($F > 8.0\sigma(F_o)$)	4898 ($F > 6.0\sigma(F_o)$)
abs cor	N/A	N/A	N/A
		Solution and Refinement	
system used		Nicolet SHELXTL PLUS (MicroVAX II)	
solution		direct methods	
refinement method		full matrix least-squares	
quantity minimized		$\sum w(F_o - F_c)^2$	
hydrogen atoms		riding model, fixed isotropic U	
final R_{obs}, %	R = 6.99	R = 7.17	R = 10.37
	R_w = 9.90	R_w = 9.76	R_w = 12.72
R_{all}, %	R = 12.48	R = 13.80	
	R_w = 12.48	R_w = 16.27	
goodness-of-fit	1.33	0.74	2.78
data/param ratio	12.7:1	7.6:1	14.3:1

4 H), 3.50 (s, 12 H). ^{13}C NMR (75 MHz, CD_3OD:D_2O {50:50}) δ 148.9, 142.8, 127.3, 126.4, 125.3, 76.3, 35.1; IR (mineral oil) 3320, 3100, 2920, 2850, 1280, 1145 cm^{-1}. MS (EI, 70 eV), *m/e* (%): 459 (15), 458 (M$^+$, 31), 440 (14), 377 (18), 376 (40), 295 (19), 294 (26), 293 (18), 267 (12), 265 (12), 191 (60), 185 (19), 169 (29), 168 (12), 157 (16), 156 (13), 109 (46), 98 (32), 96 (18), 83 (47), 82 (100), 81 (22), 55 (12), 54 (28). HRMS for $C_{24}H_{27}N_8O_2$: calcd, 459.2257; found, 459.2236.

(*E*)-1,1,4,4-Tetrakis(1-methylimidazol-2-yl)-2-buten-1,4-diol (6). To a stirred solution of 1-methylimidazole (1.3 mL, 16 mmol) in THF (20 mL) at –78 °C was slowly added *n*-butyllithium (1.6 M in hexanes, 9.7 mL, 15 mmol). After 15 min of stirring at –78 °C, diethyl fumarate (0.465 g, 2.7 mmol) was added, and the reaction mixture was allowed to stir for 8 h at room temperature. Aqueous K_2CO_3 solution (5%, 20 mL) was added, and the reaction mixture was extracted with ethyl acetate until no additional product appeared in the extracts as determined by thin layer chromatography. The combined organics were dried over K_2CO_3 and concentrated in vacuo. The crude product was recrystallized by dissolving in warm chloroform and layering with hexanes (0.375 g, 34%). Mp: 197 °C (dec). ^{1}H NMR (300 MHz, CD_3OD): δ 7.04 (d, J = 0.9 Hz, 4 H), 6.84 (d, J = 1.0 Hz, 4 H), 6.62 (s, 2 H), 3.53 (s, 12 H). ^{13}C NMR (125 MHz, DMSO-d_6): δ 147.3, 129.9, 125.1, 123.2, 73.1, 34.0. IR (KBr): 3340, 3130, 3111, 2749, 1485, 1285, 1262, 1110, 1007 cm^{-1}. MS (CI, CH_3OH/NBA), *m/e* (%): 410 (25), 409 (MH$^+$, 100), 327 (27), 246 (10), 245 (50), 228 (8), 217 (12), 201 (8), 191 (13), 177 (9), 163 (20), 155 (22), 139 (10), 138 (26), 137 (44), 135 (10), 109 (18). HRMS for $C_{20}H_{25}N_8O_2$: calcd, 409.2100; found, 409.2077.

1,1,4,4-Tetrakis(1-methylimidazol-2-yl)-1,4-butanediol (7). To a well-stirred solution of 1-methylimidazole (4.2 mL, 53 mmol) in dry THF (50 mL) at –78 °C was added *n*-butyllithium (1.6 M in hexanes, 31 mL, 50 mmol). After 15 min at –78 °C, freshly distilled diethyl succinate (1.7 mL, 10 mmol) was added, and the reaction mixture was allowed to stir 8 h at room temperature. Aqueous K_2CO_3 solution (5%, 50 mL) was then added, and the reaction mixture was extracted with $CHCl_3$ (3 × 75 mL). The combined organics were washed with water (75 mL) and dried with K_2CO_3, and the solvent was partially removed in vacuo, producing **7** as a white solid which was collected by filtration. The remaining solution was concentrated in vacuo to yield more crude **7**. Recrystallization ($CHCl_3$/layered with hexanes) yielded several crops of **7** (3.08 g total, 75%). Mp: 219.5–220 °C. ^{1}H NMR (300 MHz, CD_3OD): δ 6.98 (d, J = 0.9 Hz, 4 H), 6.83 (d, J = 1.0 Hz, 4 H), 3.49 (s, 12 H), 2.54 (s, 4 H). ^{13}C NMR (75 MHz, CD_3OD): δ 149.8, 126.2, 124.6, 74.3, 34.6, 34.5. IR (KBr): 3104, 3013, 2978, 2749, 1482, 1285, 1232, 1089, 995 cm^{-1}. MS (CI, NH_3, 70 eV), *m/e* (%): 412 (10), 411 (MH$^+$, 39), 330 (11), 329 (51), 313 (6), 248 (15), 247 (100), 246 (4), 218 (4), 192 (12), 191 (60), 190 (9), 189 (9), 165 (12), 137 (18), 109 (10), 95 (4), 84 (6), 82 (43). Anal. Calcd for $C_{20}H_{26}N_8O_2$: C, 58.52; H, 6.38; N, 27.30. Found: C, 58.14; H, 6.55; N, 26.82.

Tritiation of 7. To a suspension of **7** (37.8 mg, 0.092 mmol) in THF (15 mL) at –78 °C was added *t*-butyllithium (1.7 M in pentane, 1.9 mL, 3.23 mmol). After warming to room temperature, the reaction mixture was stirred until the solution became clear (approximately 5–10 min). Tritiated water (1 Ci/g, 0.083 mL, 4.6 mmol) was then added, and the reaction mixture was stirred for 15 min at room temperature. The mixture was diluted with aqueous K_2CO_3 solution (5% w/v, 10 mL) and extracted with chloroform (4 × 5 mL). The combined organics were washed with aqueous saturated NaCl solution (2 × 5 mL) and dried over K_2CO_3. Solvent was evaporated under a stream of nitrogen, and the resulting solid was recrystallized by dissolving in chloroform and layering with

hexanes to give white crystals of [^{3}H]-**7** (30 mg, 79% yield, 32.9 Ci/mol, 91% exchange). ^{1}H NMR data matched that of **7**.

1,1,5,5-Tetrakis(1-methylimidazol-2-yl)-1,5-pentanediol (8). Following the procedure previously employed for the preparation of **6**, 1-methylimidazole (1.3 mL, 16 mmol) was treated with *n*-butyllithium (1.6 M in hexanes, 9.7 mL, 15 mmol), followed by diethyl glutarate (0.508 g, 2.7 mmol) to yield **8** (0.481 g, 42%). Mp: 156.5–158 °C. ^{1}H NMR (300 MHz, CD_3OD): δ 6.96 (s, 4 H), 6.82 (s, 4 H), 3.45 (s, 12 H), 2.49 (br t, J = 8.1 Hz, 4 H), 1.36–1.26 (m, 2 H). ^{13}C NMR (125 MHz, CD_3OD): δ 149.7, 125.4, 124.5, 74.5, 40.9, 34.5, 19.3. IR (KBr): 3420, 2950, 1490, 1280, 1110, 1085 cm^{-1}. MS (EI, 70 eV), *m/e* (%): 424 (M^+, 6), 342 (4), 234 (11), 233 (10), 192 (15), 191 (100), 177 (5), 151 (11), 137 (6), 125 (5), 124 (5), 110 (9), 109 (50), 110 (9), 107 (5), 96 (13), 95 (6), 83 (34), 82 (49), 81 (14), 55 (7), 54 (20), 52 (5). HRMS for $C_{21}H_{29}N_8O_2$: calcd, 425.2413; found, 425.2397.

1,1,6,6-Tetrakis(1-methylimidazol-2-yl)-1,6-hexanediol (9). To a well-stirred solution of 1-methylimidazole (4.2 mL, 53 mmol) in dry THF (50 mL) at –78 °C was added *n*-butyllithium (1.6 M in hexanes, 31 mL, 50 mmol). After 15 min at –78 °C, diethyl adipate (2.0 mL, 10 mmol) was added and the reaction mixture was allowed to stir 8 h at room temperature, resulting in formation of a white precipitate. Aqueous K_2CO_3 solution (5%, 75 mL) was added, and volatile components were removed at aspirator pressure. Water (200 mL) was added, and the mixture was extracted with $CHCl_3$ (2 × 75 mL). At this point, a large amount of white precipitate was suspended in the aqueous layer. Concentrated HCl was added until all of the precipitate had dissolved. Neutralization with aqueous K_2CO_3 solution resulted in precipitation of **9**, which was collected by filtration, washed with water, air dried, and dried in vacuo. (3.54 g, 81%). Mp: 229.5–230 °C. ^{1}H NMR (300 MHz, CD_3OD): δ 6.98 (d, J = 0.9 Hz, 4 H), 6.85 (br s, 4 H), 3.40 (s, 12 H), 2.42 (br t, J = 6.8 Hz, 4 H), 1.29–1.24 (m, 4 H). ^{13}C NMR (125 MHz, CD_3OD): δ 149.8, 126.4, 124.5, 74.1, 41.1, 34.3, 24.5. IR (KBr): 3399, 3108, 2961, 2862, 1481, 1467, 1282, 1206, 1149, 1093, 1051, 987 cm^{-1}. MS (CI, NH_3, 70 eV), *m/e* (%): 439 (M^+, 13), 358 (8), 357 (34), 276 (11), 275 (62), 218 (6), 193 (6), 192 (12), 191 (65), 165 (6), 151 (13), 137 (12), 125 (9), 124 (10), 109 (26), 96 (12), 95 (5), 84 (14), 83 (67), 82 (100), 81 (12), 55 (7), 54 (11). HRMS for $C_{22}H_{31}N_8O_2$: calcd, 439.2570; found, 439.2582.

1,1,7,7-Tetrakis(1-methylimidazol-2-yl)-1,7-heptanediol (10). To a well-stirred solution of 1-methylimidazole (1.1 mL, 13.8 mmol) in dry THF (20 mL) at –78 °C was added *n*-butyllithium (1.6 M in hexanes, 8.1 mL, 13.0 mmol). After 15 min at -78 °C, a solution of diethyl pimelate (0.50 mL, 2.3 mmol) in THF (5 mL) was added, and the reaction mixture was allowed to stir for 8 h at room temperature. Aqueous K_2CO_3 (5%, 10 mL) was added; the precipitate was collected by vacuum filtration, rinsed with a small amount of cold ethyl acetate, air dried, and dried in vacuo to produce **10** (0.503 g, 49%). Mp: 159–160 °C. ^{1}H NMR (300 MHz, CD_3OD): δ 6.98 (d, J = 0.9 Hz, 4 H), 6.85 (d, J = 1.0 Hz, 4 H), 3.39 (s, 12 H), 2.45-2.38 (m, 4 H), 1.32–1.20 (m, 6 H). ^{13}C NMR (125 MHz, CD_3OD): δ 149.8, 126.4, 124.5, 74.0, 40.9, 34.3, 30.6, 24.5. IR (KBr): 3392, 3108, 2951, 2928, 1490, 1481, 1476, 1283, 1118 cm^{-1}. MS (CI, NH_3, 70 eV), *m/e* (%): 454 (16), 453 (MH^+, 58), 372 (11), 371 (46), 289 (19), 205 (9), 192 (17), 191 (100), 177 (4), 109 (13), 96 (4), 83 (49), 82 (20). HRMS for $C_{23}H_{33}N_8O_2$ (MH^+): calcd, 453.2726; found, 453.2744. Anal. Calcd for $C_{23}H_{32}N_8O_2 \cdot 0.5H_2O$: C, 59.85; H, 7.21; N, 24.28. Found: C, 59.91; H, 7.08; N, 24.10.

Tritiation of 10. To a well-stirred suspension of **10** (23.0 mg, 0.051 mmol) in THF (8 mL) at –78 °C was added a solution of *t*-butyllithium (1.7 M in pentane, 1.2 mL, 2.04 mmol). The reaction mixture was warmed to room temperature and allowed to stir until the solution became clear (approximately 5 min). Tritiated water (1 Ci/g, 0.100 mL, 5.56 mmol) was then added, and the mixture was stirred for 15 min at room temperature. An aqueous K_2CO_3 solution (5% w/v, 5 mL) was added, and the reaction mixture was extracted with chloroform (5 × 6 mL). The combined organics were washed with water (3 × 5 mL) and dried over K_2CO_3. Solvent was evaporated under a stream of nitrogen, and the resulting solid was recrystallized by dissolving in chloroform and layering with hexanes to give white crystals of [^{3}H]-**10** (10 mg, 43%, 16.6 Ci/mol, 46% exchange). ^{1}H NMR data matched that of the original compound **10**.

1,1,12,12-Tetrakis(1-methylimidazol-2-yl)-1,12-dodecanediol (11). Following the procedure previously employed for the preparation of **6**, 1-methylimidazole (1.3 mL, 16 mmol) was treated with *n*-butyllithium (1.6 M in hexanes, 9.7 mL, 15 mmol), followed by diethyl dodecanoate (0.746 g, 2.7 mmol) to yield **11** (1.34 g, 95%). Mp: 140–141.5 °C. ^{1}H NMR (300 MHz, $CDCl_3$): δ 6.93 (s, 4 H), 6.78 (s, 4 H), 5.40 (s, 2 H), 3.28 (s, 12 H), 2.49–2.44 (m, 4 H), 1.21–1.16 (m, 16 H). ^{13}C NMR (125 MHz, $CDCl_3$): δ 147.8, 125.7, 123.3, 71.7, 38.4, 33.4, 29.5, 22.6. IR (KBr): 3246, 2925, 2851, 1492, 1460, 1343, 1280, 1096, 931 cm^{-1}; MS (CI, CH_3OH/NBA), *m/e* (%): 524 (27), 523 (MH^+, 85), 442 (11), 441 (38), 439 (11), 423 (28), 360 (25), 359 (100), 357 (18), 345 (9), 205 (17), 192 (33), 191 (58), 189 (25), 187 (11), 177 (28), 137 (14), 125 (16), 109 (47), 107 (14). HRMS for $C_{28}H_{43}N_8O_2$: calcd, 523.3509; found, 523.3532.

Diethyl (3aα,6aα)-octahydro-3a,6a-dimethyl-2,5-pentalenedicarboxylic Acid (13). A solution of diene diester **12**[18] (mixture of isomers, 1.65 g, 5.9 mmol), in methanol (25 mL) was shaken for 12 h under H_2 (50 psi) in a Parr hydrogenator in the presence of 10% palladium on carbon (0.19 g). The catalyst was removed by filtration through Celite and washed with methanol. The combined filtrates were concentrated in vacuo and chromatographed on silica gel to give diesters **13**, an inseparable mixture of isomers, as a light yellow oil (1.55 g, 93%). ^{1}H NMR of mixture (300 MHz, $CDCl_3$): δ 3.84–3.73 (m, 4 H), 2.67–2.35 (m, 2 H), 1.86–1.28 (m, 8 H), 0.93 (t, J = 7.1 Hz, 6 H), 0.73 (s), 0.70 (s), 0.65 (s) (total integration for the singlets at 0.73, 0.70, and 0.65 = 6 H). ^{13}C NMR (75 MHz, $CDCl_3$): δ 175.3, 174.5, 174.4, 59.3, 52.0, 50.3, 49.8, 45.0, 44.6, 44.0, 41.9, 41.4, 41.0, 40.7, 39.4, 23.8, 23.3, 21.2, 13.6. IR (film): 2953, 2871, 1738, 1727, 1465, 1449, 1373, 1267, 1244, 1183, 1135, 1039, 863 cm^{-1}. MS (DCI, NH_3), *m/e* (%): 300 ($M + NH_4^+$, 85), 283 (MH^+, 100), 282 (39), 254 (19), 237 (32), 236 (32), 209 (26), 208 (30), 162 (22), 135 (35), 108 (20). HRMS for $C_{16}H_{26}O_4$ ($M+NH_4^+$): calcd, 300.2175; found, 300.2176.

(2α,3aβ,5α,6aβ)-, (2α,3aα,5α,6aα)-, and (2α,3aα,5β,6aα)-Octahydro-2,5-bis(1-methylimidazol-2-yl)hydroxymethyl)-3a,6a-dimethylpentalene (14–16). To a well-stirred solution of 1-methylimidazole (5.31 g, 64.8 mmol) in THF (50 mL) at –78 °C was added *n*-butyllithium (1.6 M in hexanes, 38.8 mL, 62.1 mmol). After 15 min at –78 °C, the diester **13** (mixture of isomers, 3.0 g, 10.8 mmol) in THF (10 mL) was added. After 1 h at –78 °C, the reaction mixture was warmed to room temperature and stirred for 16 h. After the addition of aqueous K_2CO_3 (5% w/v, 50 mL), volatile components were removed in vacuo. To the residue was added more aqueous K_2CO_3 (5% w/v, 100 mL), and the resulting mixture was extracted with chloroform (4 × 125 mL). The organic extracts were washed with water (2 × 125 mL), dried over K_2CO_3, and concentrated in vacuo to give a viscous yellow residue (8.4 g), which was recrystallized in several crops (chloroform, layered with hexanes), with each crop yielding a single diastereomer: **14** (0.5 g, 9%), **15** (3.6 g, 64%), and **16** (0.3 g, 5%). The ratio **14**:**15**:**16** varied considerably from run to run. Isomer **14** showed a 5.7% NOE enhancement from the methyl singlet at δ 0.98 to the methine pentet at δ 3.59.

(2α,3aβ,5α,6aβ)-Octahydro-2,5-bis(1-methylimidazol-2-yl)hydroxymethyl)-3a,6a-dimethylpentalene (14). Mp: 233.5–234 °C. ^{1}H NMR (300 MHz, $CDCl_3$): δ 6.91 (s, 4 H), 6.73 (s, 4 H), 5.49 (s, 2 H), 3.59 (pentet, J = 9.3 Hz, 2 H), 3.36 (s, 12 H), 1.96 (dd, J = 13.1, 9.4 Hz, 4 H), 1.34 (dd, J = 13.1, 9.3 Hz, 4 H), 0.98 (s, 6 H). ^{13}C NMR (75 MHz, $CDCl_3$): δ 148.0, 125.5, 123.1, 73.0, 51.2, 44.2, 39.8, 33.8, 22.6. IR (KBr): 3411, 3107, 2956, 2939, 2867, 1491, 1459, 1449, 1406, 1343, 1285, 1145, 1073, 953, 943 cm^{-1}. MS (CI, NH_3, 70 eV), *m/e* (%): 521 (6), 520 (32), 519 (100), 438 (13), 437 (46), 421 (4), 356 (21), 354 (6), 328 (7), 327 (4), 245 (5), 205 (4), 192 (13), 191 (76), 177 (4), 176 (4), 109 (5). HRMS for $C_{28}H_{39}N_8O_2$ (MH^+): calcd, 519.3196; found, 519.3202. Anal. Calcd for $C_{28}H_{38}N_8O_2 \cdot H_2O$: C, 62.67; H, 7.51; N, 20.88. Found: C, 62.35; H, 7.07; N, 20.48.

(2α,3aα,5α,6aα)-Octahydro-2,5-di(1-methylimidazol-2-yl)hydroxymethyl)-3a,6a-dimethylpentalene (15). Mp: 221.5–222 °C. ^{1}H NMR (300 MHz, $CDCl_3$): δ 6.92 (d, J = 0.8 Hz, 4 H), 6.76 (s, 4 H), 5.38 (s, 2 H), 3.66 (pentet, J = 9.4 Hz, 2 H), 3.40 (s, 12 H), 1.66–1.57 (m, 8 H), 0.94 (s, 6 H). ^{13}C NMR (75 MHz, $CDCl_3$): δ 148.0, 125.4, 123.3, 72.8, 49.8, 43.2, 41.5, 33.8, 24.1. IR (KBr): 3409, 2954, 2946, 2864, 1490, 1340, 1321, 1281, 1101, 1087, 933 cm^{-1}. MS (CI, NH_3, 70 eV), *m/e* (%): 520 (5), 519 (MH^+, 13), 438 (5), 437 (20), 356 (10), 355 (44), 354 (9), 328 (4), 289 (9), 245 (12), 217 (5), 192 (18), 191 (100), 149 (3), 83 (25), 82 (8), 55 (4), 54 (6), 42 (8). Anal. Calcd for $C_{28}H_{38}N_8O_2$: C, 64.84; H, 7.38; N, 21.60. Found: C, 64.47; H, 7.33; N, 21.45.

(2α,3aα,5β,6aα)-Octahydro-2,5-di(1-methylimidazol-2-yl)hydroxymethyl)-3a,6a-dimethylpentalene (16). Mp: 177–178 °C. ^{1}H NMR (300 MHz, $CDCl_3$): δ 6.92 (s, 2 H), 6.90 (d, J = 0.9 Hz, 2 H), 6.75 (s, 2 H), 6.73 (d, J = 0.9 Hz, 2 H), 5.53 (s, 1 H), 5.36 (s, 1 H), 3.71–3.42 (m, 2 H), 3.392 (s, 6 H), 3.389 (s, 6 H), 1.86 (t, J = 11.9 Hz, 2 H), 1.67–1.57

(18) Camps, P.; Iglesias, C.; Rodríguez, M. J.; Desamparados Grancha, M.; Gregori, M. E.; Lozano, R.; Miranda, M. A.; Figueredo, M.; Linares, A. *Chem. Ber.* **1988**, *121*, 647–654.

(m, 2 H), 1.49–1.37 (m, 4 H), 0.99 (s, 6 H). ^{13}C NMR (125 MHz, CD_3OD): δ 149.44, 149.36, 126.32, 126.26, 124.63, 124.55, 74.8, 74.6, 45.5, 43.9, 43.8, 43.3, 34.39, 34.31, 25.1. IR (KBr): 3392, 3105, 2949, 2866, 1490, 1341, 1332, 1282, 1143, 1096, 941 cm^{-1}; MS (CI, CH_3OH/NBA), *m/e* (%): 520 (29), 519 (MH^+, 84), 438 (12), 437 (36), 435 (16), 419 (22), 356 (24), 355 (100), 353 (23), 337 (11), 327 (10), 273 (10), 255 (11), 245 (26), 243 (9), 213 (8), 205 (9), 203 (9), 193 (8), 192 (44), 191 (83), 189 (10), 187 (10), 178 (9), 177 (51), 176 (20), 161 (10), 154 (13), 149 (8), 137 (18), 136 (14), 133 (8), 121 (10), 109 (91), 107 (18). HRMS for $C_{28}H_{39}N_8O_2$: calcd, 519.3196; found, 519.3205.

Tritiation of 14. To a well-stirred suspension of **14** (26.0 mg, 0.049 mmol) in THF (2 mL) at −78 °C was added *t*-butyllithium (1.7 M in pentane, 1.0 mL, 1.72 mmol). The reaction mixture was warmed to room temperature and stirred until the solution became clear (approximately 5–10 min). Tritiated water (1 Ci/g, 0.062 mL, 3.44 mmol) was then added and the reaction mixture was stirred 15 min at room temperature. The mixture was diluted with aqueous K_2CO_3 (5% w/v, 5 mL) and extracted with chloroform (5 × 6 mL). The combined organics were washed with water (3 × 5 mL) and dried over K_2CO_3. After the solvent was evaporated under a stream of nitrogen, the remaining solid was recrystallized by dissolving in chloroform and layering with hexanes to give white crystals of [^{3}H]-**14** (5.5 mg, 22% yield, 23.4 Ci/mol, 65% exchange). NMR data matched that of the original **14**.

Tritiation of 15. To a well-stirred suspension of **15** (23.0 mg, 0.044 mmol) in THF (1.5 mL) at −78 °C was added *t*-butyllithium (1.7 M in pentane, 0.90 mL, 1.54 mmol). The reaction mixture was warmed to room temperature and stirred until the solution became clear (approximately 5–10 min). Tritiated water (1 Ci/g, 0.055 mL, 3.08 mmol) was then added and the solution was stirred 15 min at room temperature. The mixture was diluted with aqueous K_2CO_3 solution (5% w/v, 5 mL) and extracted with chloroform (3 × 15 mL). The combined organics were washed with water (2 × 10 mL) and dried over K_2CO_3. Solvent was evaporated under a stream of nitrogen, and the residue was dried 15 min under vacuum. The product was recrystallized by dissolving in chloroform and layering with hexanes to give white crystals of [^{3}H]-**15** (10.6 mg, 47% yield, 18.9 Ci/mol, 53% exchange). ^{1}H NMR data matched that of the original **15**.

(3aα,6aα)-Octahydro-2,5-bis(bis(1-methylimidazol-2-yl)methylene)-3a,6a-dimethylpentalene (17). To a stirred solution of diol **15** (0.72 g, 1.39 mmol) in pyridine (10 mL) at 0 °C under nitrogen was added thionyl chloride (0.507 mL, 6.9 mmol). After being stirred for 30 min at 0 °C, the reaction was warmed to room temperature, stirred for 30 min, quenched with aqueous K_2CO_3, and extracted with CH_2Cl_2. The organic layer was dried over $MgSO_4$, filtered, and concentrated in vacuo. The crude product (orange-brown oil) was filtered through a plug of silica gel and then crystallized from CH_3CN to give 0.16 g (23% yield) of diene **17**. Mp: 220–225 °C. ^{1}H NMR (300 MHz, $CDCl_3$): δ 7.00 (s, 4 H), 6.74 (s, 4 H), 3.20 (s, 12 H), 2.75 (d, *J* = 19.2 Hz, 4 H), 2.54 (d, *J* = 19.4 Hz, 4 H), 0.97 (s, 6 H). ^{13}C NMR (125 MHz, $CDCl_3$): δ 157.3, 145.5, 127.7, 120.6, 113.8, 50.0, 45.2, 32.8, 21.1. IR (KBr): 3105, 2959, 2951, 1491, 1466, 1458, 1451, 1406, 1280, 1137, 953, 887, 750, 735, 690, 676 cm^{-1}. MS (CI, CH_3OH/NBA), *m/e* (%): 484 (34), 483 (100), 482 (9), 268 (7), 267 (23), 253 (7), 216 (7), 201 (9), 176 (11). HRMS for $C_{28}H_{35}N_8$: calcd, 483.2985; found, 483.2977.

Isolation of Crystals of $[Ni_2(15)_2Cl]Cl_3 \cdot 8H_2O$ (18). A solution of **15** (100 mg, 0.2 mmol) in MeOH (5 mL) was combined with a solution of Ni(dimethoxyethane)Cl_2[19] (88 mg, 0.4 mmol) in MeOH (10 mL) in a 25-mL round-bottom flask. The solution immediately turned purple. After 1 h the solution was concentrated to about 5 mL by evaporation of solvent with heating. The flask was then connected by a glass tube to a 25-mL round-bottom flask containing diethyl ether (15 mL) and placed in the refrigerator at 2–6 °C. No attempt was made to exclude water during the crystallization. After 1 week, purple crystals of suitable size for X-ray crystal structure analysis were isolated. Selection of the appropriate crystals was performed in a 50% MeOH/diethyl ether solution, as evaporation of solvent of crystallization caused decomposition of the crystals. Selected crystals were mounted on the end of glass fibers with epoxy cement. The mounted crystals were dipped into epoxy to completely seal the crystal from solvent loss. Details of the crystal data are given in Table I. Positional parameters, selected bond lengths and selected bond angles are provided in Tables II and III (see supplementary material).

Isolation of Crystals of $[Ni_2(9)_2(NO_3)(H_2O)_2](NO_3)_3 \cdot 2H_2O$ (19). A suspension of **9** (100 mg, 0.2 mmol) in water (10 mL) was slowly acidified with 0.1 M HNO_3 until the solid had dissolved. To the acidified solution was added $Ni(NO_3)_2 \cdot 6H_2O$ (120 mg, 0.4 mmol). The resulting solution was slowly made alkaline with 1 M NaOH until the solution became dark purple (approximately pH 8). The water was allowed to evaporate, and the purple residue was dissolved in methanol (10 mL). Crystallization occurred by vapor diffusion of diethyl ether into the methanol solution at 4 °C, as described for **18**. Once suitable crystals for X-ray diffraction analysis formed, several were isolated as described for **18**. These crystals were also sensitive to loss of crystallization solvent. Selected crystals were encased in epoxy cement on the end of glass fibers. Details of the crystal data are given in Table I. Positional parameters, selected bond lengths, and selected bond angles are provided in Tables IV and V (see supplementary material).

Isolation of Crystals of $[Ni_2(7)_2(NO_3)(H_2O)_2](NO_3)_3 \cdot 3H_2O$ (20). To a solution of $Ni(NO_3)_2$ (0.188 g, 0.65 mmol) in H_2O (5 mL) was added the tetraimidazole **7** (0.133 g, 0.32 mmol). The reaction mixture was gently heated and swirled until all of the solid had dissolved, during which time the solution became deep blue in color. Slow evaporation at room temperature produced **20** as purple crystals (0.161 g, 78%). Details of the crystal data are given in Table I. Positional parameters, selected bond lengths and selected bond angles are provided in Tables VI and VII (see supplementary material). Mp: 120–250 °C dec. IR (KBr): 3364 (br), 1493, 1384, 1314, 1283, 742 cm^{-1}. Anal. Calcd for $C_{40}H_{62}N_{20}Ni_2O_{21}$: C, 37.64; H, 4.90; N, 21.95, Ni, 9.20. Found: C, 37.86; H, 4.65; N, 22.13, Ni, 9.57.

Gel Electrophoresis Studies. Plasmid DNA experiments were conducted at room temperature. Supercoiled plasmid pUB110[20] or pSP64-(polyA)[21] (4500 base pairs) was reconstituted using HPLC grade water and stored frozen until needed. DNA solutions were made up in 10 μM EPPS (4-(2-hydroxyethyl)-1-piperazinepropanesulfonic acid) buffer at pH 8.0. Reaction solutions were made by adding a solution of plasmid DNA to a solution of metal–ligand complex, also in EPPS buffer. The final concentration of DNA was 25 μg/mL (~40 μM in base pairs), 10 μL total volume. To all reactions were added 2 μL of bromophenol blue–xylene cyanole–50% glycerol stain immediately before loading onto the gel.[16] Electrophoresis was carried out on 1% agarose gels containing ethidium bromide (0.5 μg/mL). Electrophoresis buffer contained 0.08 M TRIS–phosphate, pH 7.5. Where noted, a 2.0 mM solution of ethylenediaminetetraacetic acid (EDTA) was also added to the buffer. However, in most experiments, EDTA was not used in order to eliminate the possibility of complexation of EDTA to the transition metal being studied. Gels were run at 60–75 V for 45–90 min.

When electrophoresis was carried out with radiolabeled ligands, each lane was cut into five pieces. Each piece was rinsed with distilled water and placed in a scintillation vial. To each vial was added 1–2 mL of water, and the vials were capped and heated overnight in an oven at 95 °C to melt and dissolve the agarose pieces. The vials were allowed to cool, filled with Ecolume scintillation cocktail, and counted for ^{3}H in a scintillation counter.

Metal Concentration Dependence NMR Experiments. Metal concentration dependence NMR experiments were performed at 300 or 500 MHz in MeOH-d_4 by adding aliquots of $Zn(NO_3)_2 \cdot 6H_2O$ in MeOH-d_4 to the ligand dissolved in MeOH-d_4. Spectra were acquired 5 min after each addition. Stacked plots obtained from these experiments feature the imidazole *N*-methyl region. Due to the slow rate of metal exchange at room temperature and below, separate resonances were observed for each complex present. The *N*-methyl signal was analyzed in detail because its chemical shift was most sensitive to metal ion binding. In addition, it is a singlet in a region of the spectrum relatively free of other signals.

Procedure for Ultrafiltration Binding Studies. All solutions were prepared in EPPS buffer (10 mM) at pH 8. Centricon C-100 ultrafilters were used. These filters have a 100,000 molecular weight cutoff. Filters with a lower molecular weight cutoff were tried, but were unacceptable because the ligands showed a significant amount of binding to the membranes in the presence of Ni(II). Highly polymerized calf thymus DNA was sonicated for 20 h to fragment it into smaller pieces and solubilize it in water. To the upper reservoir of a Centricon C-100 filter was added 0.5 mL of a solution of calf thymus DNA (usual [DNAP] = 2.5 mM) followed by 0.5 mL of a premixed solution of radiolabeled ligand and metal salt. Solutions were mixed using a vortex mixer and spun for 30 min at 3000 rpm in a Sorvall RC2-B centrifuge at room temperature, and the collected filtrate was set aside. The retentate was collected by backspinning the filters at 1000 rpm for 10 min. Samples of the filtrate

(19) Ward, L. G. L. *Inorg. Synth.* **1972**, *13*, 160–162.

(20) Gryczan, T. J.; Contente, S.; Dubnau, D. *J. Bacteriol.* **1978**, *134*, 318–329.

(21) Marrot, L.; Leng, M. *Biochemistry* **1989**, *28*, 1454–1461.

Table VIII. ^{1}H NMR Data for Ligands **4**, **6**, **7**, **8**, **9**, **10**, **11**, **14**, and **15**

ligand	freq, MHz	solvent	resonances, ppm (multiplicity, integration)
4	300	$CDCl_3$	2.06 (s, 3H), 3.28 (s, 6H), 5.68 (s, 1H), 6.82 (s, 2H), 6.96 (s, 2H)
	300	CD_3OD	1.99 (s, 3H), 3.50 (s, 6H), 6.86 (s, 2H), 7.03 (s, 2H)
6	300	DMSO-d_6	6.29 (s, 2H), 6.75 (s, 4H), 7.11 (s, 4H)
7	300	$CDCl_3$	2.72 (s, 4H), 3.56 (s, 12H), 6.71 (s, 4H), 6.80 (s, 4H), 8.50 (br s, 2H)
8	300	$CDCl_3$	1.42 (m, 4H), 2.53 (t, 2H, J = 7.9 Hz), 3.32 (s, 12H), 5.54 (s, 2H), 6.77 (s, 4H), 6.91 (s, 4H)
9	300	DMSO-d_6	1.12 (br m, 4H), 2.26 (br m, 4H), 3.27 (s, 12H), 5.74 (s, 2H), 6.76 (s, 4H), 7.03 (s, 4H)
10	300	$CDCl_3$	1.20 (m, 4H), 1.33 (m, 2H), 2.48 (m, 4H), 3.30 (s, 12H), 5.34 (s, 2H), 6.80 (s, 4H), 6.94 (s, 4H)
11	300	$CDCl_3$	1.22 (br m, 16H), 2.50 (m, 4H), 3.30 (s, 12H), 5.41 (s, 2H), 6.81 (s, 4H), 6.96 (s, 4H)
14	300	$CDCl_3$	1.00 (s, 6H), 1.37 (m, 4H), 1.97 (m, 4H), 3.38 (s, 12H), 3.61 (m, 2H), 5.52 (s, 2H), 6.75 (s, 4H), 6.93 (s, 4H)
	500	CD_3OD	1.10 (s, 6H), 1.39 (m, 4H), 1.87 (m, 4H), 3.41 (s, 12H), 3.52 (m, 2H), 6.86 (s, 4H), 6.96 (s, 4H)
15	300	$CDCl_3$	0.97 (s, 6H), 1.62 (m, 8H), 3.41 (s, 12H), 3.65 (m, 2H), 5.42 (s, 2H), 6.78 (s, 4H), 6.95 (s, 4H)
	500	CD_3OD	0.87 (s, 6H), 1.60 (m, 4H), 1.74 (m, 4H), 3.36 (s, 12H), 3.48 (m, 2H), 6.87 (s, 4H), 6.97 (s, 4H)

and retentate (20 μL each) were analyzed for tritium by scintillation counting and for DNA by diluting and measuring UV absorbance at 260 nm (0.154 mM DNAP/absorbance unit). Control experiments were conducted by replacing DNA solutions with buffer to determine whether the radiolabeled ligands were able to pass freely through the membranes.

General Procedure for Precipitation Studies. All experiments were performed in EPPS buffer (10 mM) at pH 8. DNA stock solutions (0.3 mL, various concentrations) were placed in Eppendorf tubes to which were added 0.3 mL of a solution containing ^{3}H-labeled ligand (0.10 mM for **7**, **10**, and **14**; 0.20 mM for **4**) and $Ni(NO_3)_2$ (0.20 mM for all ligands). Tubes were vortexed and spun for 1 h in a microcentrifuge. Samples of the supernatants were diluted to appropriate levels with 10 mM EPPS buffer at pH 8 (depending upon original DNA concentration), and DNA concentration in the diluted sample was determined by UV absorbance at 260 nm (0.154 mM DNAP/abs. unit). Control experiments verified that no DNA precipitation could be observed with DNA alone, with DNA and $Ni(NO_3)_2$, or with DNA and ligand only. Spermine was tested in a similar manner, except no nickel was added. Precipitated DNA was removed by centrifugation. The supernatant was analyzed for DNA by UV absorbance measurements at 260 nm. The radiolabeled ligand concentration was determined by scintillation counting. The $Ni(NO_3)_2$ concentration was varied from 0 to 50 mM while the radiolabeled ligand concentration was held at 50 μM. The concentration of DNA was initially at 600 μM in base pairs. For the preassociation study, ligand **14** and $Ni(NO_3)_2$ (both at 2× the target concentration) were incubated 24 h at room temperature, while in the studies without preassociation, the $Ni(NO_3)_2$ was added to the DNA in the top of the filter, and mixed, and the ligand solution was added immediately before ultrafiltration.

Results

Ligand Synthesis. As part of this work, a variety of new imidazole-containing ligands were prepared. 1-Methylimidazole groups were used for metal coordination because of their similarity to the histidine residue, which is commonly coordinated to metals in enzymes. As shown below, all new ligands were prepared via the addition of excess 2-lithio-1-methylimidazole to the corresponding ester or diester. The preparation of diimidazole **4** has been described previously,[17] and the diester precursors to ligands **5–11** are all commercially available. Ligands **14–16** were prepared from diester **13**, which has previously been prepared by hydrogenation of diester diene **12**.[18] Hydrogenation of **12** with palladium on carbon gave a three-component mixture of diesters **13**. The ratio of isomers varied from run to run and appeared to depend on the time of hydrogenation and the presence of adventitious acid or base. Treatment of this mixture with 2-lithio-1-methylimidazole gave a mixture of **14**, **15**, and **16**, which could be cleanly separated and purified by recrystallization from $CHCl_3$/hexanes. The bis(olefin) **17** was prepared from any one of the three diols **14–16** via dehydration with $SOCl_2$ in pyridine.

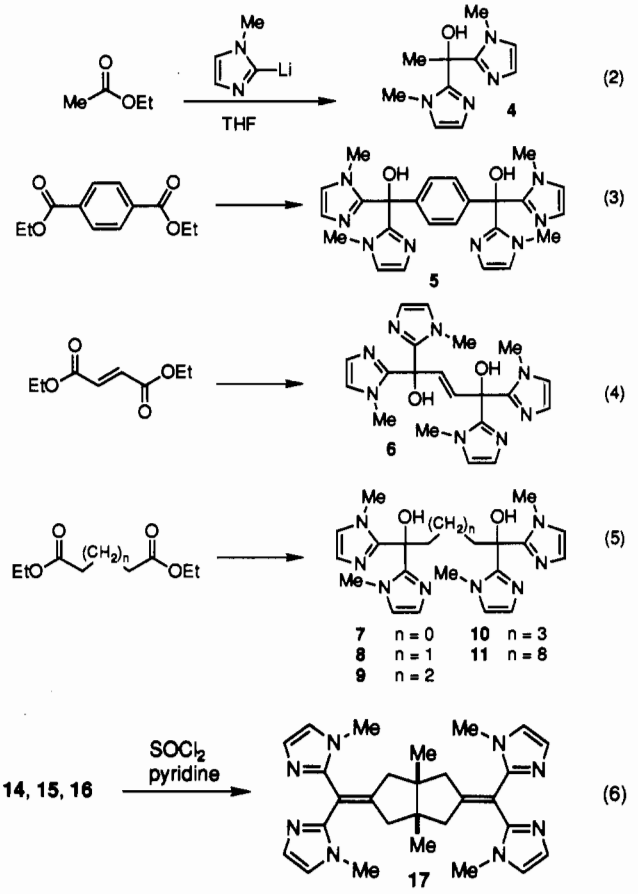

(2) (3) (4) (5) (6)

Hydrolysis of Simple Phosphate Diesters. Table IX displays the pseudo-first-order rate constants, k_0, for the hydrolysis of bis(4-nitrophenyl) phosphate by Ni(II), Cu(II), and Zn(II) complexes of ligands **4**, **9**, **14**, tris(2-aminoethyl)amine (tren), and 2,2′-bipyridine (bpy). The rate constants for the metal complexes of diimidazole ligand **4** were similar to those observed for the metal–bpy complexes. For the Cu(II) complex of **4** at pH 7.00, the observed rate enhancement was greater for $Cu(\mathbf{4})^{2+}$ than that for $Cu(bpy)^{2+}$ by a factor of approximately 2. From these studies it was clear that a dramatic rate enhancement does not occur with the binucleating ligands. Additionally, precipitation was observed, in several cases, on addition of the metal-ligand mixtures to the phosphate diester solution.

Gel Electrophoresis Studies. The Ni(II) and Zn(II) complexes of **4**, **9**, **14**, **15**, and **17** were incubated with pUB110 supercoiled plasmid DNA at ambient temperature (20–25 °C). Subsequent electrophoresis in a buffer containing 2.0 mM EDTA, which should chelate any metal cations that are free in solution or loosely bound to the DNA, produced the gel shown in Figure 1. Several of the Ni(II) and Zn(II) binucleating complexes show different migration patterns (lanes 2–4 and 6–8) than the control lane (lane 1) containing no meta–ligand complex. With the Ni(II) complex derived from **14**, the DNA was observed to remain in the well (top of figure—not visible) possibly as a result of precipitation of the metal-ligand-DNA complex. Lanes 3 and 4

Scheme I

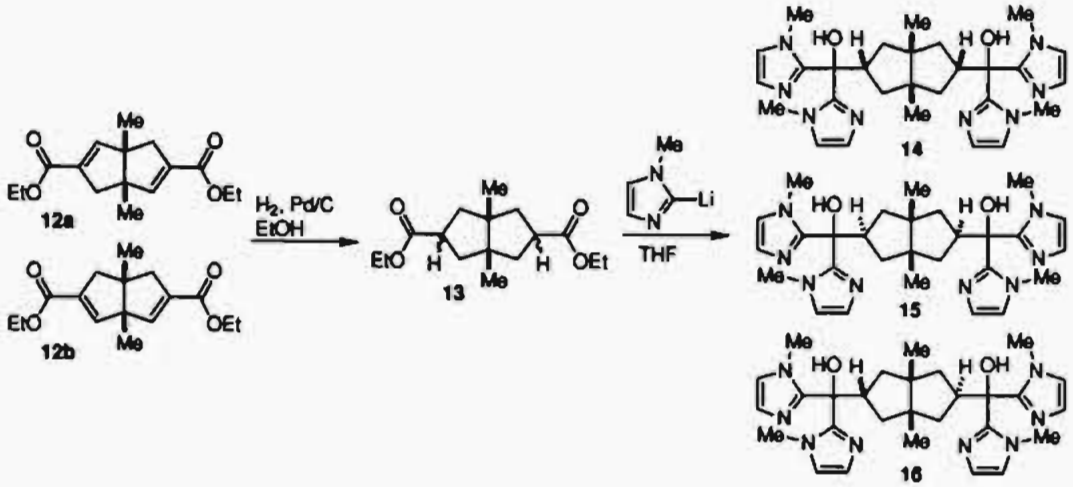

Table IX. Representative Observed Pseudo-First-Order Rate Constants, k_0, for the Hydrolysis of Sodium Bis(4-nitrophenyl) Phosphate in Water at 75 °C[a]

complex		pH 7.00		pH 8.60	pH 10.00
M^{2+}	L	10^6k_0, s^{-1} [b]	10^6k_0, s^{-1} [c]	10^6k_0, s^{-1} [c]	10^6k_0, s^{-1} [c]
Ni	**14**[e]	*d*	*d*	*d*	*d*
	9	*d*	0.12 ± 0.01	0.30 ± 0.01	3.27 ± 0.18
	4	0.95 ± 0.02	0.08 ± 0.01	0.20 ± 0.03	
	tren	0.17 ± 0.01	*f*	0.44 ± 0.07	7.80 ± 0.34
	bpy	0.46 ± 0.04	0.16 ± 0.03	0.83 ± 0.01	5.10 ± 0.20
Cu	**14**[e]	*d*	1.41 ± 0.11	0.24 ± 0.03	*d*
	9	*d*	16.1 ± 2.5	8.83 ± 0.34	
	4	21.1 ± 0.6	4.79 ± 0.58	2.31 ± 0.16	
	tren	0.05 ± 0.00	*f*	0.17 ± 0.01	4.00 ± 0.11
	bpy	13.6 ± 1.1	4.31 ± 0.21	2.78 ± 0.35	5.22 ± 0.21
Zn	**14**[e]	*d*	0.17 ± 0.00	0.08 ± 0.01	*d*
	9	*d*	0.23 ± 0.02	1.14 ± 0.04	
	4	1.46 ± 0.59[d]	0.24 ± 0.01	0.16 ± 0.02	*d*
	tren	0.05 ± 0.00	*f*	0.17 ± 0.02	3.88 ± 0.11
	bpy	1.39 ± 0.11	0.22 ± 0.02	0.25 ± 0.01	4.14 ± 0.11
control		0.026 ± 0.004		0.13 ± 0.02	3.68 ± 0.13

[a] pH measurements made at 75 °C with temperature compensation probe, μ = 0.1 M ($NaNO_3$), 0.01 M buffer; **14**, **9**, and **4** are defined in text; tren = tris(2-aminoethyl)amine, bpy = 2,2′-bipyridine, $K_w = 2.0 \times 10^{-13}$, hydrolysis values are uncorrected for spontaneous (control) hydrolysis. The control values were obtained by using identical conditions except M^{2+} and L were omitted. [b] 1.0×10^{-3} M M_nL^{2n+} concentration. [c] 1.0×10^{-4} M M_nL^{2n+} concentration. [d] Precipitates formed in these samples. [e] Solution contains 18% CH_3CN by volume to prevent precipitation of the complex. [f] Not distinguishable from control values.

with Ni(II) complexes of ligands **15** and **17**, respectively, showed "smearing" of the DNA, suggesting that the metal–ligand complex was still bound to the DNA. A similar "smearing" effect has been observed in the binding of *cis*-diamminedichloroplatinum (*cis*-DDP) to plasmid DNA.[21] The Zn(II) complexes of ligands **14**, **15**, and **17** (lanes 7–9) were also found to smear or slow the movement of the DNA during gel electrophoresis. This suggests binding of the metal–ligand complex to the DNA, though not to as great an extent as the corresponding Ni(II) complexes. No significant inhibition of gel mobility was observed for either the Ni(II) or Zn(II) complexes of the binucleating acyclic ligand **9** or the mononucleating ligand **4**.

The dependence of the gel mobility assay on metal–ligand concentration with a pSP64 plasmid and Ni(II) and Zn(II) complexes of ligand **14** is shown in Figure 2. A metal–ligand concentration of 50 μM was necessary to observe changes in gel mobility in both cases. At a concentration of 5 μM ligand (10 μM metal), no inhibition of gel mobility was observed with either Ni(II) or Zn(II). Normal gel mobility could be restored on

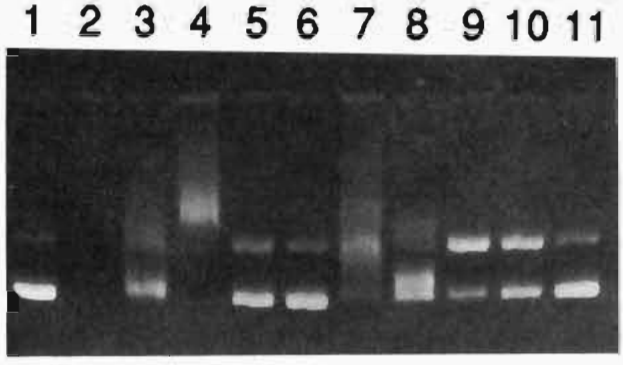

Figure 1. Reaction of tetraimidazole and diimidazole complexes of Ni(II) and Zn(II) with supercoiled pUB110 (25 μg/mL, 40 μM bp) plasmid DNA at pH 8.0 (EPPS, 10 mM) at 25 °C for 15 min. $[M_2L^{4+}] = 100$ μM, $[M(4)^{2+}] = 200$ μM. Key: lane 1, DNA control (no metal or ligand); lane 2, Ni_2(**14**); lane 3, Ni_2(**15**); lane 4, Ni_2(**17**); lane 5, Ni_2(**9**); lane 6, Ni(**4**); lane 7, Zn_2(**14**); lane 8, Zn_2(**15**); lane 9, Zn_2(**17**); lane 10, Zn_2(**9**); lane 11, Zn(**4**).

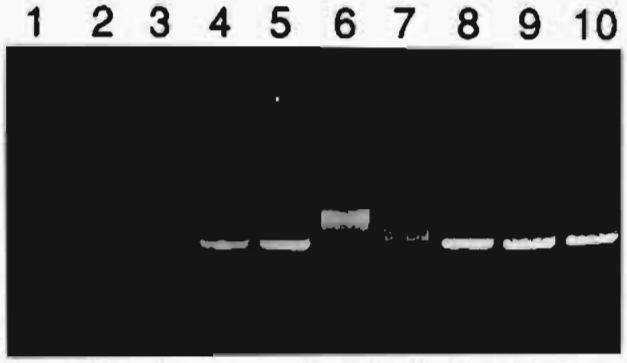

Figure 2. Gel mobility of supercoiled pSP64 (25 μg/mL, 40 μM bp, all lanes) plasmid DNA in the presence of Ni_2(**14**) and Zn_2(**14**) at pH 8.0 (EPPS, 10 mM) at 25 °C after incubation for 15 min. Key: lane 1, DNA only (no metal or ligand); lane 2, 500 μM $Ni_2(14)^{4+}$; lane 3, 50 μM $Ni_2(14)^{4+}$; lane 4, 5 μM $Ni_2(14)^{4+}$; lane 5, 0.5 μM $Ni_2(14)^{4+}$; lane 6, 500 μM $Zn_2(14)^{4+}$; lane 7, 50 μM $Zn_2(14)^{4+}$; lane 8, 5 μM $Zn_2(14)^{4+}$; lane 9, 0.5 μM $Zn_2(14)^{4+}$; lane 10, DNA only.

addition of potassium cyanide, as shown in Figure 3. This suggests that the binding interaction occurs by coordination of the metal ion to the DNA, or that the cyanide ion removes the metal ions from the ligand, which destroys the metal–ligand–DNA complex. Coordination of cyanide also will eliminate the cationic charge on the metal complexes. In previous studies of mononuclear Cu(II), Ni(II), and Zn(II) complexes we had not observed such shifts in gel mobility when they were incubated with DNA.[5l-k]

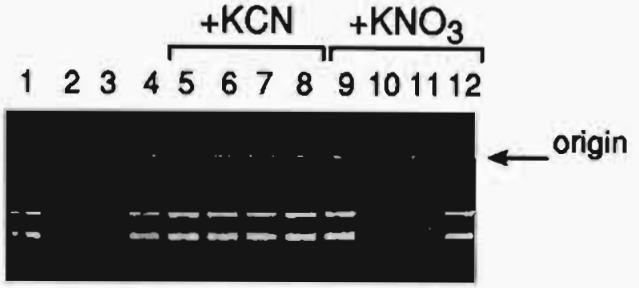

Figure 3. Reversal by KCN of mobility retardation of pSP64(poly A) plasmid DNA caused by Ni(II)–ligand complexes during electrophoresis on 1% agarose. [DNA(P)] was 50 μM in all lanes. Lanes 1–4 were control lanes (no KCN), lanes 5-8 contained 50 mM KCN, and lanes 9–12 contained 50 mM KNO_3. Ligands were present as follows: lanes 1, 5, and 9, no ligand; lanes 2, 6, and 10, **14**; lanes 3, 7, and 11, **15**; lanes 4, 7, and 12, **10**. In all lanes which contained ligand, $Ni(NO_3)_2$ was present at a concentration of 100 μM. Before addition of KCN (or KNO_3), DNA was incubated for 5 min with the premixed Ni(II):ligand solution.

Only complexes of metals with slow substitution kinetics, such as Pt(II), are expected to exhibit such an effect.[22]

The effect of binding of the Ni(II) complexes of **14**, **15**, and **17** to pUB110 plasmid DNA incubated with $NaNO_3$ or ethidium bromide was studied. The binding of Ni(II) with ligand **14** was not affected by ionic strength but was inhibited by the presence of ethidium bromide. Intercalation of ethidium bromide causes the DNA double helix to unwind, changing the base pair to base pair and the phosphate to phosphate distances, which may interfere with binding of the metal–ligand complex.[22] The Ni(II) complexes of ligands **15** and **17** were also not affected by ionic strength, but were affected by ethidium bromide. The inhibition of the binding of the nickel complexes of **15** and **17** by ethidium bromide was not as dramatic as the inhibition observed for the nickel complex of **14** because of the apparently stronger binding of the nickel complex of **14** to the DNA (see Figure 1).

NMR Experiments. In order to develop a better understanding of the solution coordination dynamics of these metal–ligand complexes in the absence of DNA, several NMR experiments were performed. Figure 4 contains the 500-MHz ^{1}H NMR spectra of ligands **14** (upper spectrum) and **15** (lower spectrum) in MeOH-d_4. A listing of the signals is presented in Table VIII. The largest resonance in each of the two spectra, near 3.4 ppm, can be attributed to the *N*-methyl signal. The location and relative intensity of this resonance provides a convenient handle to follow metal coordination to the ligands. The 300-MHz ^{1}H NMR spectrum of diimidazole **4** in MeOH-d_4 is shown in Figure 5.

Since octahedral Ni(II) is paramagnetic, and would interfere with the NMR spectrum of the ligand, the Zn(II) complex was chosen for study. Shown in Figure 6 is the 3.5–4.2 ppm region of the ^{1}H NMR spectrum of diimidazole **4** (0.10 M) in MeOH-d_4 at −80 °C with increasing amounts of $Zn(NO_3)_2$. The *N*-methyl peak, at approximately 3.6 ppm, shifts downfield with increasing zinc concentration to yield two resonances at 4.00 and 4.05 ppm, presumably from the mono- and bis(ligand) complexes **21** and **22**. The peak at 4.00 ppm is present throughout the entire titration

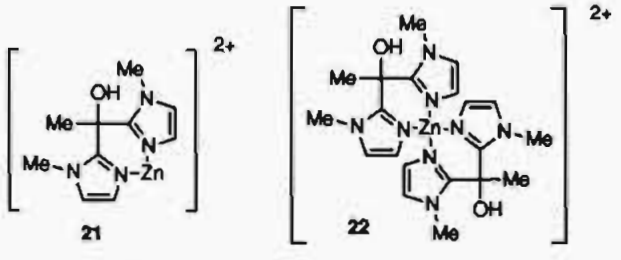

(22) For a recent discussion of DNA intercalation, see: Long, E. C.; Barton, J. K. *Acc. Chem. Res.* **1990**, *23*, 271–273.

Table X

signal	L_mZn_n	structure
a	L	
b	L_1Zn	
c	L_2Zn_2	
d	LZn	
e	LZn_2	
f	L_mZn_m (polymer)	

range of the experiment. The peak at 4.05 ppm becomes a shoulder on the downfield side of the major metal–ligand species. The major species at a 1:1 Zn:4 ratio appears to be the mono(ligand) complex, **21**. Only two species are expected to be present in this solution. No tris(ligand) complex ($Zn(4)_3$) was observed, since Zn(II) often prefers tetrahedral coordination. No species due to monodentate binding of diimidazole **4** to the metal are apparent.

The different types of possible Zn(II) complexes with ligands **14** and **15** are represented in Table X. The free ligand, denoted signal a, can be monitored as the most upfield N–CH_3 resonance at 3.4 ppm. When zinc(II) is added it decreases in intensity as the bound imidazole groups have downfield shifted N–CH_3 resonances in the 3.9–4.1 ppm region. The free ligand signal also splits somewhat because of the presence of species b and d, where only one site of the binucleating ligand is occupied by the metal. Once the upfield N–CH_3 resonance disappears, then only species such as c and e, or the polymeric form of f, can be present. The presence of oligomers or polymers of type f should produce broad NMR signals.

The ^{1}H NMR spectra of 0.01 M **15** in MeOH-d_4 at 25 °C, with concentrations of $Zn(NO_3)_2$ varying from 0–6.0 equiv, appear in Figure 7. In the initial spectrum, the free ligand, species a, appears as the upfield singlet at 3.37 ppm. With added zinc, the first dominant species to appear, a feature at 4.12 ppm can be attributed to species b, where two ligands bind a single zinc. Other minor species appear at 4.09 (species d) and 3.99 ppm (species c). On addition of further zinc to about 0.5 equiv, species b decreases in intensity as the peak at 4.09 ppm gains intensity and a new broad resonance grows in near the same position. The broad feature f dominates through 1.0 equiv of zinc and is attributed to various oligomers and polymers expected for species f. Further increasing the zinc concentration beyond 1.0 equiv, results in the formation of a new resonance at 4.03 ppm. This becomes dominant in the final spectrum with 6.0 equiv of added zinc and is attributed to species e. The peak at 3.99 ppm persists over a wide concentration range. Because of the similar chemical shift to e, it is assigned to species c. The weak feature at 3.94 ppm that only appears between 0.4 and 0.7 equiv of added zinc is puzzling. Given the complexity of the system, and the possible additional complications from the formation of zinc hydroxy species, the assignments are regarded as tentative. The assign-

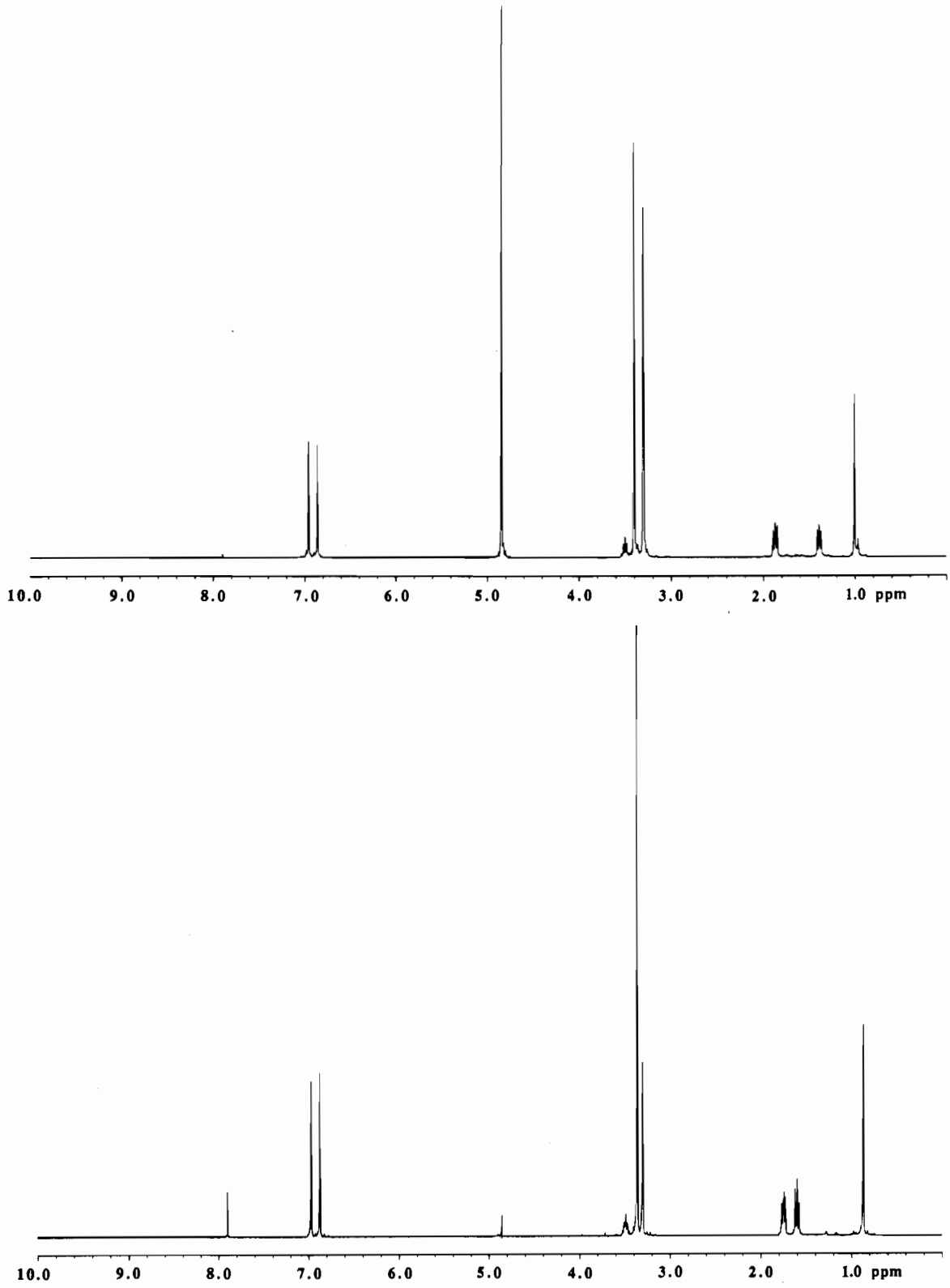

Figure 4. ^{1}H NMR (500 MHz) spectra of **14** (upper spectrum) and **15** (lower spectrum) in MeOH-d_4 at 25 °C.

ments for species b and e, the limiting cases, are the firmest.

Figure 8 contains spectra for a similar NMR experiment with ligand **14**. Because of lower solubility, the concentration of ligand was reduced to 0.005 M. Initially, species b can be attributed to the resonance at 4.19 ppm with 0.2 equiv of added zinc. This disappears and a new sharp resonance grows in slightly upfield at 4.18 ppm with further added zinc. This peak disappears soon and resembles the behavior of species d of ligand **15**. A peak appears at 3.93 ppm with 0.4 equivalents of added zinc(II), and dominates at higher concentrations of zinc, when the upfield free N–CH_3 resonance at 3.4 ppm has disappeared. This suggests that it be assigned to the 2:2 complex, species c. Beyond 1.0 equiv of added zinc, many other broad features appear that might represent oligomers or polymers denoted by species f. At high zinc concentrations the spectrum begins to simplify with one dominant species at 4.09 ppm that can be attributed to species e. These studies confirm that the ligand cannot chelate all four imidazoles to one metal. Molecular models suggest that the octahydropentalene spacer does not have enough conformational flexibility to accommodate this structure. At the maximum metal

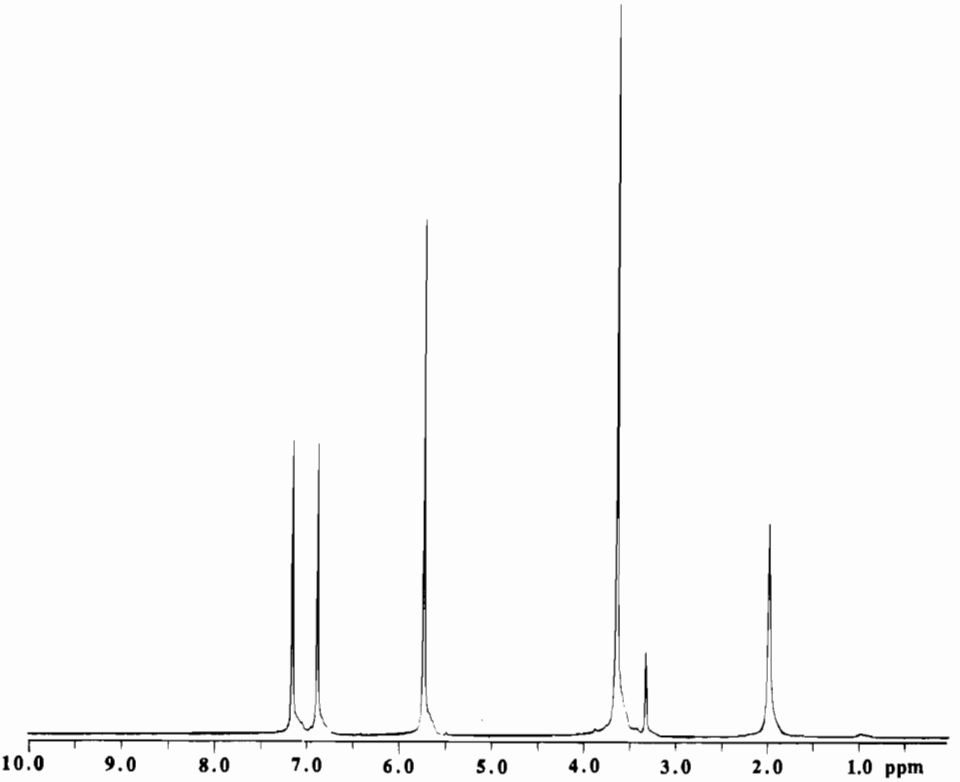

Figure 5. ^{1}H NMR (300 MHz) spectrum of **4** in MeOH-d_4 at −80 °C.

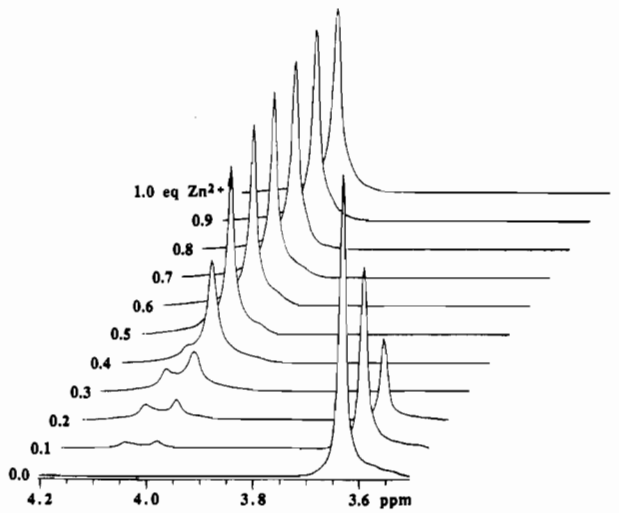

Figure 6. Stacked plot of the ^{1}H NMR (300 MHz) spectra of **4** in MeOH-d_4 at −80 °C by titration with $Zn(NO_3)_2$ from 0 to 1.0 equiv of Zn(II) to **4**.

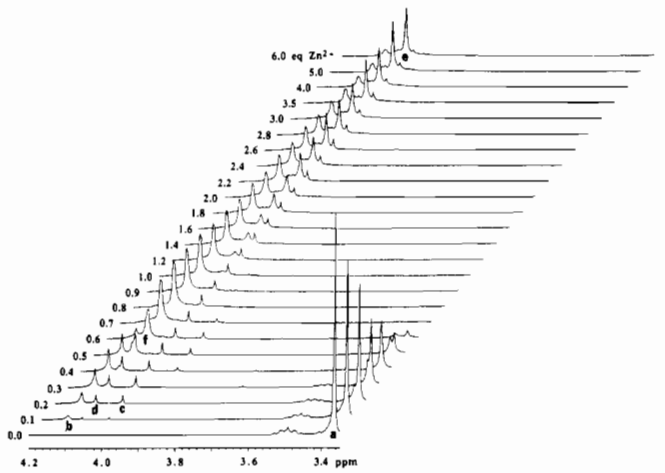

Figure 7. Stacked plot of the ^{1}H NMR (500 MHz) spectra of **15** in MeOH-d_4 at 25 °C by titration with $Zn(NO_3)_2$ from 0 to 6.0 equiv of Zn(II) to **15**.

ion concentration, the 2:1 Zn–**15** complex (signal e, 4.03 ppm) was the major species in solution.

The most important observation from this series of studies is that at 2 equiv of Zn(II) to **15**, the 2:1 species (signal e) is one of the major species in solution (see Figure 9). If the DNA binding process involves the metal ion, the 2:1 metal–ligand complex with Zn(II) would be expected to be the active species in DNA binding.

A comparison of the results from the titration experiments of **14** and **15** suggests a possible explanation for the stronger DNA binding activity of the metal complexes of **14**. With 2 equiv of metal to ligand (Figure 9), the primary species with ligand **14** was the 2:1 complex, e, which we postulate to be the active DNA binding species. With ligand **15** at the same metal to ligand ratio (Figure 9), a larger percentage of the metal–ligand complex appears to be in other forms. Since the 2:1 complex, e, is postulated to be the active form of the DNA binding agent, this might partially explain the enhanced binding of **14**.

Metal Complexes. In order to further develop our understanding of the coordination environment of the metal–ligand complexes involved in DNA binding, these ligands were combined with Ni(II) and Zn(II) under a variety of conditions. Crystalline products could be isolated in several cases and were characterized by X-ray crystallography.

Treatment of the 1,6-hexanediol derivative **9** with $Ni(NO_3)_2 \cdot 6H_2O$ in H_2O produced a bimetallic complex **19** with the formula $[Ni_2(\mathbf{9})_2(NO_3)(H_2O)_2](NO_3)_3$ that was recrystallized from MeOH/Et_2O and analyzed by X-ray crystallography. An ORTEP diagram of **19** is shown in Figure 10. Each Ni(II) center is octahedral but contains different coordination environments. Ni(1) is coordinated to four imidazoles, two from each equivalent of the ligand, and two water molecules (O(5) and O(6)), while Ni(2) binds to four imidazoles, two from each equivalent of ligand, and one bridging nitrate (O(7)–N(17)–O(8)). The Ni–Ni

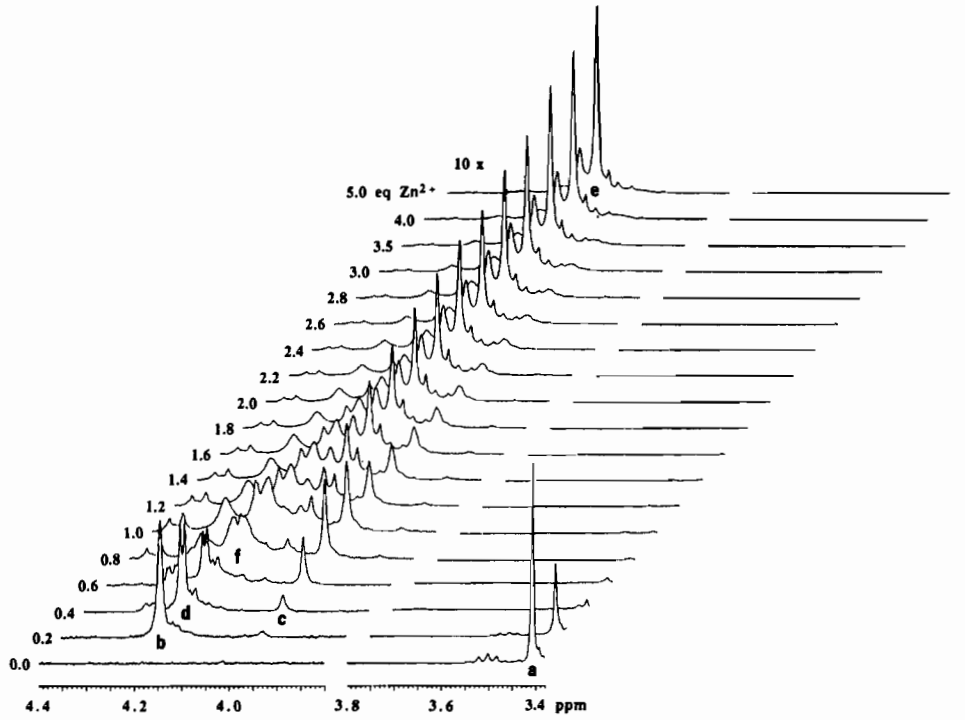

Figure 8. Stacked plot of the ^{1}H NMR (500 MHz) spectra of **14** in MeOH-d_4 at 25 °C by titration with $Zn(NO_3)_2$ from 0 to 5.0 equiv of Zn(II) to **14**.

separation is 9.48 Å. This large distance suggests that there is no cooperativity between the two metal centers. To balance the charge, a pocket of uncoordinated nitrate ions and water molecules is present, as shown in the crystal packing diagram (Figure 11). Two water molecules, represented by O(14) and O(15), exist as 50% occupancy (O(14a) and O(15a)) sites. Hydrogen bonding in the crystal is shown in Figure 11 and the crystal structure data parameters are listed in Table I. Atomic coordinates are listed in Table II and selected bond lengths and angles are provided in Table III (see supplementary material).

All of the Ni-N bond lengths of **19** are in the range 2.02–2.08 Å. The distances are typical for octahedral Ni(II) complexes.[23] The two water molecules on Ni(1) are equidistant from the metal (2.16 Å) but the two Ni(II) to nitrate oxygen bonds are significantly different, 2.26 Å for Ni(2)–O(8) and 2.14 Å for Ni(2)–O(7). This suggests that O(8) of the nitrate binds considerably less strongly than O(7). The asymmetrically bridging nitrate causes the O(7)–Ni(2)–O(8) bond angle to be 57.5°.

The ligand–Ni–ligand bond angles associated with O(5), O(6), N(1), and N(7) are considerably distorted from the 90° bond angles of a perfectly octahedral structure. For example, the N(1)–Ni(1)–N(7) bond angle is 103.3°. The other angles around the equatorial plane are all collapsed slightly below 90° with the smallest angle being 83.6° for O(5)–Ni(1)–O(6). This is not surprising since the water molecules (O(5) and O(6)) are the most flexible ligands associated with the metal center.

The equatorial plane around Ni(2) defined by O(7), O(8), N(11), and N(15) is also distorted away from a normal square plane. As mentioned previously, the nitrate bond angle of O(7)–Ni(2)–O(8) is acute at 57.5°. The other three angles around the equatorial plane are all above 90°. As for Ni(1), the largest angle is that which points to the "inside" of the molecule, N(11)–Ni(2)–N(15), at 108.2°. The movement of the nitrogen atoms around Ni(2) toward the nitrate may be the cause of the lengthening of the Ni(2)–O(8) bond and the small O(7)–Ni(2)–O(8) bond angle. The two equatorial planes around Ni(1) and Ni(2) deviate from each other by 15°.

Treatment of ligand **15** with Ni(dimethoxyethane)Cl_2[19] in MeOH gave a complex with the molecular formula $[Ni_2(\mathbf{15})_2Cl]Cl_3$ (**18**). Recrystallization from MeOH/Et_2O gave crystals of **18** suitable for characterization by X-ray crystallography. An ORTEP diagram of **18** is presented in Figure 12. Atomic coordinates for **18** are listed in Table IV and selected bond lengths and bond angles are provided in Table V (see supplementary material). With ligand **15** the nitrate derivative did not give material suitable for analysis by X-ray crystallography. The two nickel atoms in **18** are bridged by a single chloride (Cl(1)) which leads to a Ni–Ni through bond distance of 4.76 Å. Unlike **19**, both Ni centers adopt a distorted trigonal bipyramidal geometry with each nickel being coordinated to four imidazoles, two from each equivalent of ligand, and the bridging chloride.

The Ni(1)–Cl(1) bond length 2.386(3) Å and the Ni(2)–Cl(1) bond length 2.378(3) Å, are equivalent within experimental error. The Ni(1)–Cl(1)–Ni(2) bond angle is 173.7° which deviates somewhat from the expected 180° angle. The Ni–N bond lengths to both Ni(1) and Ni(2) are all between 1.98 and 2.01 Å, which is only slightly shorter than the Ni–N bonds in complex **19** (2.02–2.08 Å). All Ni–N bond lengths lie in the range for normal Ni(II)–N bonds in trigonal bipyramid structures.[20]

The N(1)–Ni(1)–N(9) bond angle in the equatorial plane is 100.6°. This is less than the expected 120.0° angle for a nondistorted trigonal bipyramid structure. The N(9)–Ni(1)–Cl(1) angle of 138.3° compensates for this. The N(1)–Ni(1)–Cl(1) angle is 121.2°, close to the expected value. The axial N–Ni(1)–equatorial N angles are all near the expected value of 90° with the interligand N–Ni(1)–N angles (for example N(1)–Ni(1)–N(3)) above 90° and the intraligand N–Ni(1)–N angles (for example N(1)–Ni(1)–N(3)) angles slightly below 90°. A similar effect is observed for the inter- and intraligand N–Ni(2)–N angles.

The outside angle on Ni(2) (N(7)–Ni(2)–N(15)) is 99.2°, similar to the outside angle on Ni(1). The angle N(7)–Ni(2)–Cl(1), opposite N(9)–Ni(1)–Cl(1) (138.3°), is 134.3°, whereas, the angle N(15)–Ni(2)–Cl(1), opposite N(1)–Ni(1)–Cl(1)

(23) Saconi, L.; Mani, F.; Bencini, A. In *Comprehensive Coordination Chemistry: The Synthesis, Reactions, Properties, and Applications of Coordination Compounds*; Wilkinson, G., Ed.; Pergamon Press: New York, 1987; Vol. 5, Chapter 50.

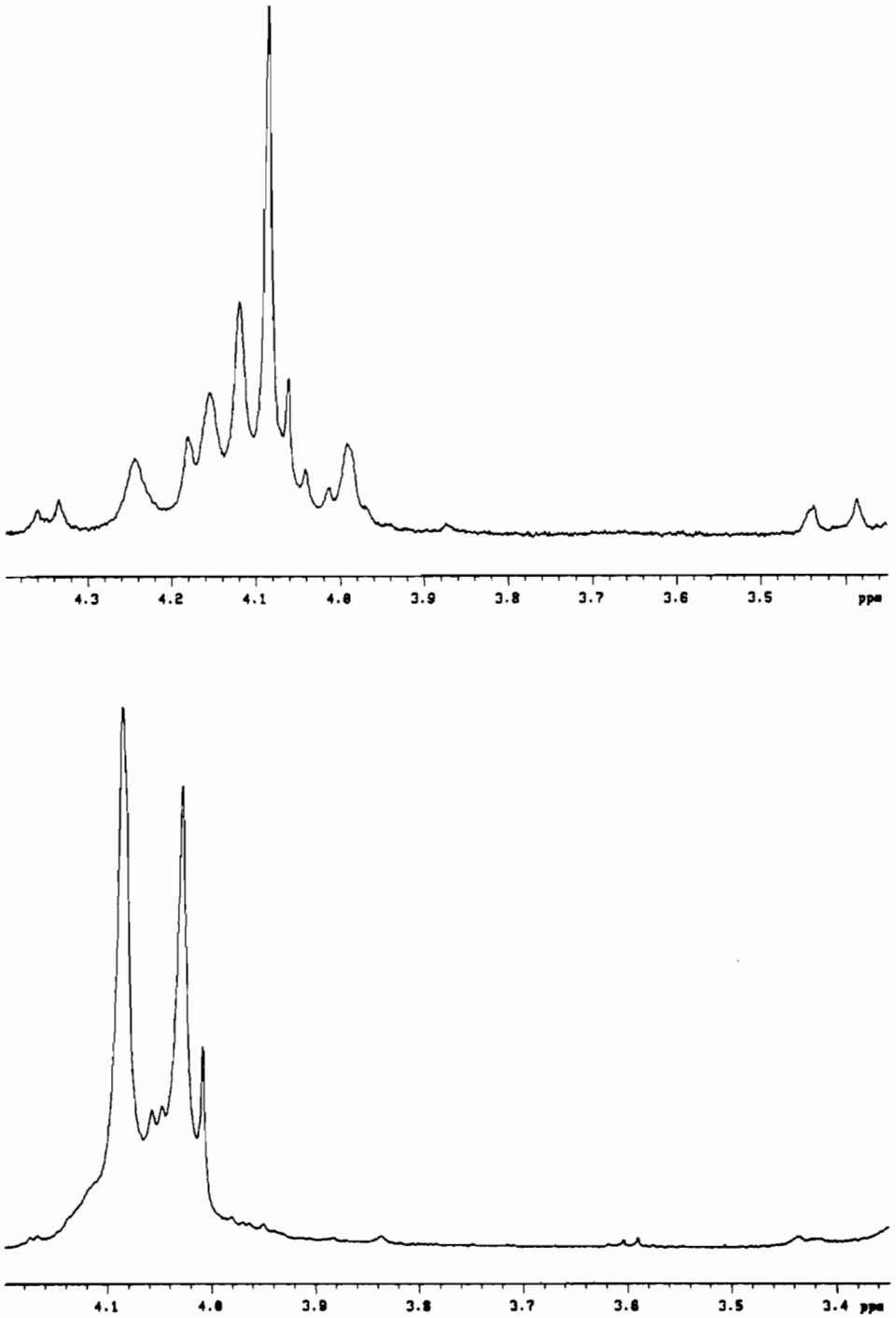

Figure 9. *N*-Methylimidazole region of the ^{1}H NMR (500 MHz) spectra of 2 equiv of Zn(II) with ligands **14** (upper spectrum) and **15** (lower spectrum).

(121.2°) is 126.4°. This makes a pseudo-C_2 rotation axis about Cl(1) in the vertical direction through the plane defined by N(1), N(9), N(7), and N(15). Bond angles around the two metal centers are represented in Figure 13.

Treatment of the 1,4-butanediol derivative **7** with aqueous $Ni(NO_3)_2$ produced the bimetallic complex **20** with the formula $[Ni_2(\mathbf{7})_2(NO_3)(H_2O)_2](NO_3)_3$. Slow evaporation of solvent at room temperature gave crystals suitable for X-ray analysis. An ORTEP diagram of **20** is shown in Figure 14. The structure is very similar to **19**. The Ni–Ni distance in complex **20** is 7.51 Å, over 2 Å shorter than in **19**. Unlike complex **19**, the nitrate oxygen to Ni(2) distances are also nearly equal, with Ni(2)-O(5) at 2.22 Å and Ni(2)–O(6) at 2.18 Å. Also, as in **19**, the O(5)–Ni(2)–O(6) bond angle is 57.5°. The charge is balanced by three uncoordinated nitrate ions; three poorly defined water molecules are also present in the crystal lattice. Crystal structure data parameters are shown in Table I. Atomic coordinates are listed in Table VI, and selected bond lengths and angles are listed in Table VII (see supplementary material).

Preparation of Radiolabeled Ligands. In order to study the binding of these metal/ligand complexes to DNA in more detail, it was necessary to prepare ligands that were radiolabeled. Radiolabeling was readily accomplished with **4**, **7**, **10**, **14**, and **15** by deprotonation of the 1-methylimidazole groups at the 5-position with *t*-butyllithium, followed by addition of tritiated water (eq 2). *t*-Butyllithium was found to be a much more effective polylithiating agent than *n*-butyllithium. The alcohol was also deprotonated and tritiated in this process but was converted to the protonated form on treatment with H_2O. To determine the optimum conditions for tritium incorporation into the imidazole system, studies were first performed with a D_2O quench to determine the minimum amount of tritiated water necessary for

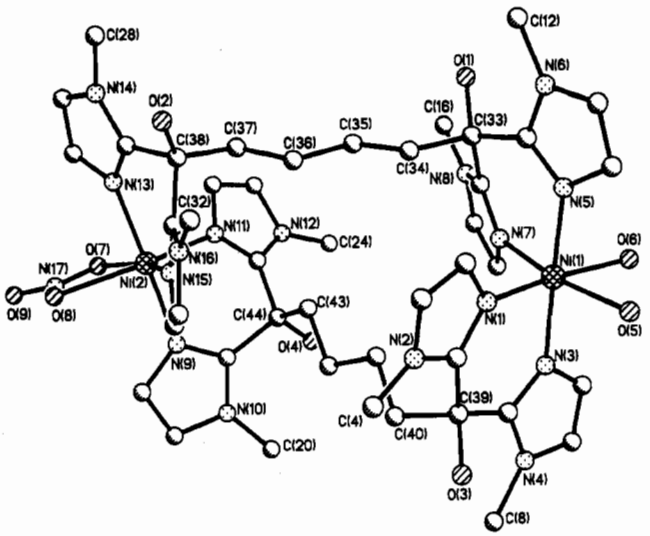

Figure 10. Ball and stick representation of $[Ni_2(\mathbf{9})_2(NO_3)(H_2O)_2](NO_3)_3 \cdot 2H_2O$ ($\mathbf{19} \cdot 2H_2O$), showing the atom labeling scheme. Nitrate counter ions have been omitted for clarity.

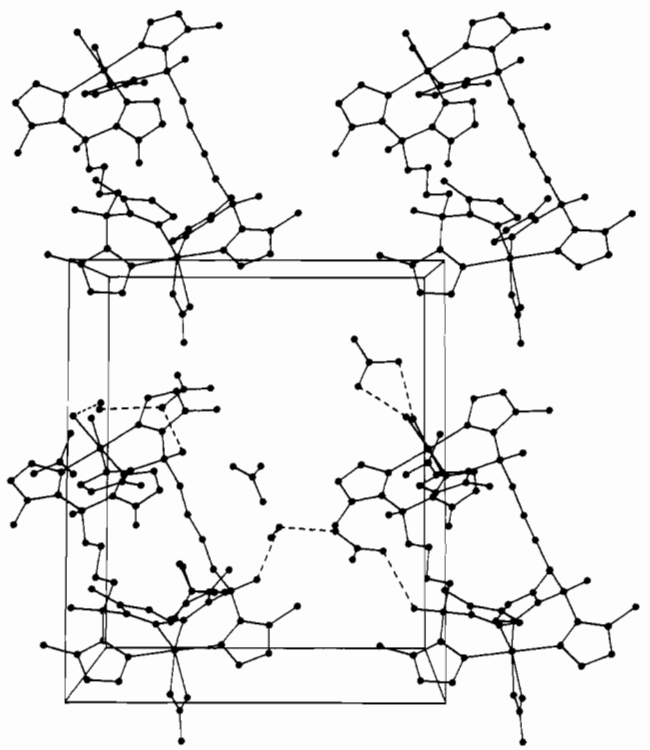

Figure 11. Packing diagram of $[Ni_2(\mathbf{9})_2(NO_3)(H_2O)_2](NO_3)_3(\mathbf{19} \cdot 2H_2O)$, showing the hydrogen bonding in the crystal (along the *a* axis).

efficient labeling. In theory, only 6 equiv of base are required to deprotonate the two alcohols and the four 1-methylimidazoles in the tetraimidazole ligands. However, in practice, 30 equiv or more of *t*-butyllithium were necessary to achieve 60–80% exchange. The extent of deuterium incorporation was determined by analysis of the ^1H NMR spectrum. It was found that each compound required slightly different amounts of base and aqueous quench to achieve optimal exchange. Details of each labeling study are presented in Tables XI–XIV (see supplementary

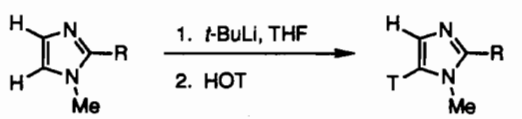

(7)

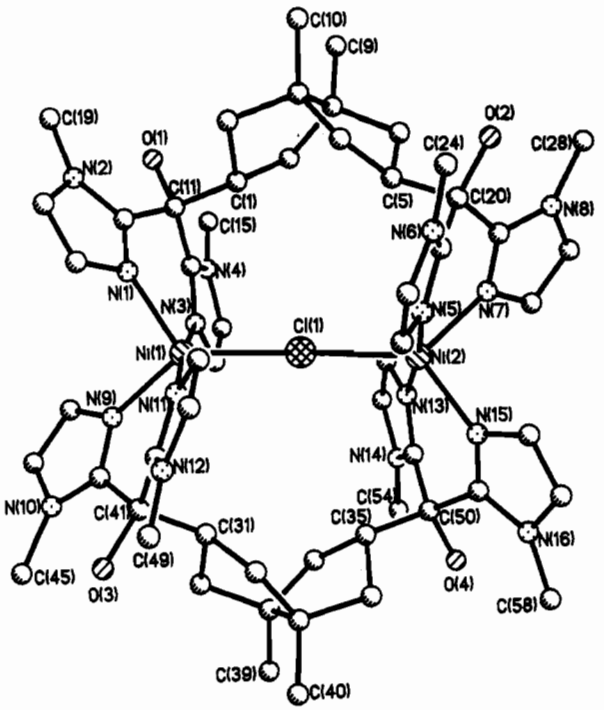

Figure 12. Ball and stick representation of $[Ni_2(\mathbf{15})_2Cl]Cl_3 \cdot 8H_2O$ ($\mathbf{18} \cdot 8H_2O$), showing the atom labeling scheme. Chloride counter ions and solvent molecules have been omitted for clarity.

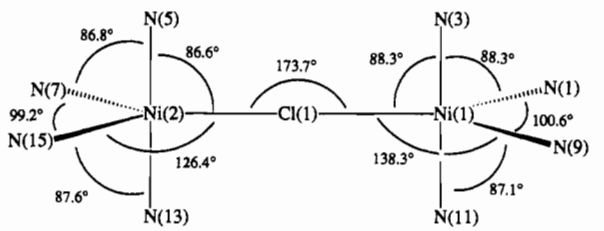

Figure 13. Representative view of the atom positions around the metal centers from the X-ray crystal structure of **18** showing the pseudotrigonal bipyramidal geometry about Ni(II).

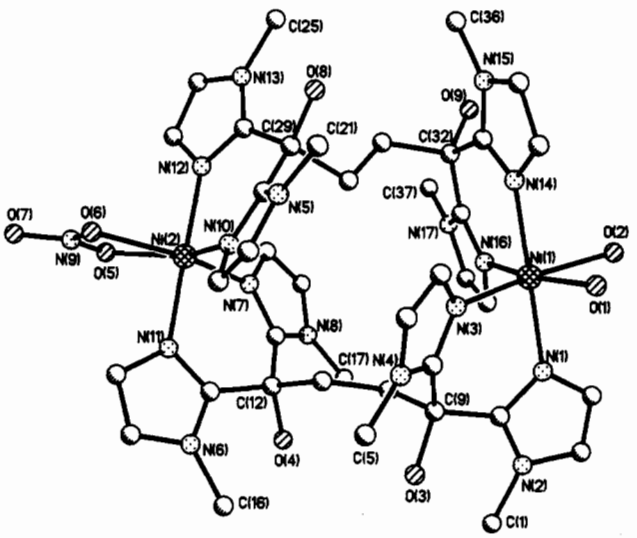

Figure 14. Ball and stick representation of $[Ni_2(\mathbf{7})_2(NO_3)(H_2O)_2](NO_3)_3 \cdot 3H_2O$, ($\mathbf{20} \cdot 3H_2O$), showing the atom labeling scheme. Nitrate counter ions and solvent molecules have been omitted for clarity.

material). Using this technique, **4**, **7**, **10**, **14**, and **15** were labeled with tritium to levels of approximately 5 Ci/mol of methylimidazole.

Agarose gel electrophoresis was carried out using the radiolabeled ligands [^3H]-**4**, [^3H]-**10**, [^3H]-**14**, and [^3H]-**15** with Ni-

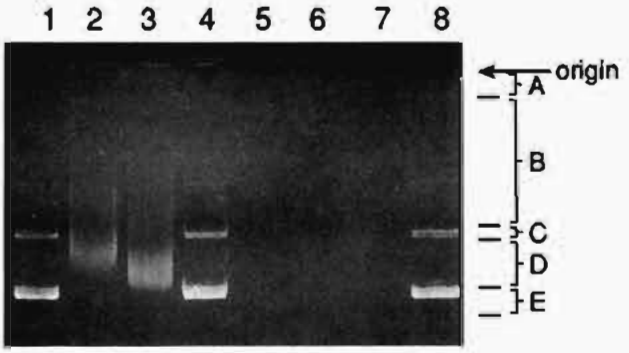

Figure 15. Gel cutting diagram, showing the location of slices. Electrophoresis of pSP64(poly A) plasmid DNA on 1.4% agarose in the presence of varying concentrations of **15**. Lanes 1–4 and lane 8 contained DNA at 50 μM in base pairs. Lanes 5–7 contained no DNA. Concentration of **15** as follows: lanes 2 and 5, 500 μM; lanes 3 and 6, 50 μM; lanes 4 and 7, 5 μM; lanes 1 and 8, 0 μM. Concentration of $Ni(NO_3)_2$ was twice the concentration of **15** in all cases.

Table XV. Radioactivity in Slices of Gel from Figure 16[a]

	lane							
slice	1	2	3	4	5	6	7	8
A	189	240	159	82	192	135	111	70
B	46	129	106	68	73	60	63	52
C	30	31	33	28	32	43	30	31
D	33	36	32	34	33	32	33	35
E	32	32	34	29	35	40	29	29

[a] All values are counts per minute of tritium.

(II) as previously described. Gels were run with plasmid pSP64(poly A). No EDTA was used in the electrophoresis buffer.

To determine if the ligands were migrating with the DNA, each gel lane was cut into five pieces, and each piece was checked for the presence of radiolabeled ligand. Figure 15 shows a diagram of the gel cutting experiment conducted with [^{3}H]-**14** and [^{3}H]-**15**. Counting data for this gel are shown in Table XV. The lines in Figure 15 indicate the manner in which the gel was sliced for analysis. Gel slices which contained the DNA (slices C and D) had only background levels of radioactivity and therefore had no ligand bound to the DNA. Gel slices located closer to the origin (slices A and B) did contain ligand, but in amounts similar to that found in the control lanes. These results suggest that the ligands, if indeed bound to the DNA, dissociate from the DNA as it migrates through the gel.

Ultrafiltration Binding Studies. Initial attempts to measure DNA binding by equilibrium dialysis failed because the metal reagents bind strongly to dialysis membranes. Centricon filters were investigated to provide another assay for DNA binding.[24] In this procedure, the DNA and radiolabeled binding agent are added to a chamber above the filter, and the solution is passed through the filter with the assistance of centrifugation. Only the free ligand and metal can pass through the size selective filter, while the macromolecular DNA and metal/ligand/DNA complex are retained in the top chamber.

Results of representative ultrafiltration experiments are shown in Table XVI. The diimidazole ligand **4** showed only a very small amount of binding while all of the tetraimidazole ligands showed relatively high levels of binding.

The effect of ionic strength was tested by studying the binding of the Ni(II)–**14** complex to DNA in the presence of increasing amounts of mono-, di-, and tetracations. Figure 16 shows the effect of added NaCl on the binding of the **14**–Ni(II) complex to DNA. The binding of the complex remained constant even

(24) (a) Sophianopoulos, J. A.; Durham, S. J.; Sophianopoulos, A. J.; Ragsdale, H.L; Cropper, Jr., W. P. *Archiv. Biochem. Biophys.* **1978**, *187*, 132–37. (b) Smoluk, G. D.; Fahey, R. C.; Ward, J. F. *Radiat. Res.* **1988**, *114*, 3–10. (c) Grover, N.; Gupta, N.; Thorp, H. H.; *J. Am. Chem. Soc.* **1992**, *114*, 3390-93.

Table XVI. Ultracentrifugation Binding Studies[a]

ligand	metal	DNA (+/–)	^{3}H CPM in filtrate	% of total ligand bound
14	Ni(II)	–	19 541 ± 1632	97
		+	602 ± 252	
	Zn(II)	–	26 835 ± 542	91
		+	2303 ± 421	
15	Ni(II)	–	17 034 ± 1547	72
		+	5183 ± 1702	
	Zn(II)	–	19 082 ± 320	97
		+	730 ± 186	
10	Ni(II)	–	15 625 ± 195	92
		+	1395 ± 207	
	Zn(II)	–	3043 ± 93	88
		+	368 ± 5.4	
7	Ni(II)	–	30 588 ± 367	97
		+	894 ± 39	
	Zn(II)	–	1000 ± 39	86
		+	141 ± 8.3	
4	Ni(II)	–	22 527	16
		+	18 379	
	Zn(II)	–	27 188 ± 227	1
		+	26 971 ± 370	

[a] DNA starting concentration was 600 μM in base pairs, metal ion concentrations were 100 μM (as the nitrates) and ligand concentrations were as follows: **14**, **15**, and **10**, 50 μM; **4**, 100 μM. Percentage of total ligand bound was calculated based on radioactivity in filtrates of blank runs done without DNA.

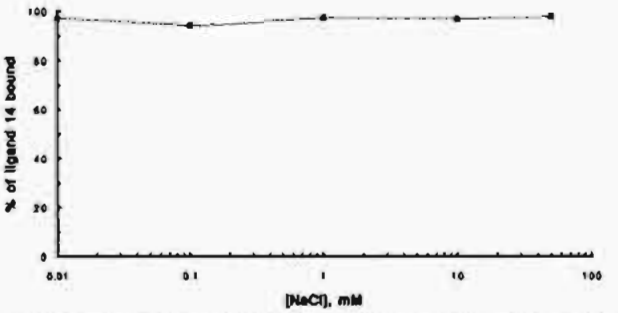

Figure 16. Effect of increasing [NaCl] on binding of **14** to DNA in the presence of $Ni(NO_3)_2$. Concentrations were as follows: [DNA(P)], 1.2 mM; [**14**], 50 μM; $Ni(NO_3)_2$, 100 μM. Order of addition to the ultrafiltration device was: DNA, NaCl, and **14**–$Ni(NO_3)_2$ mixture.

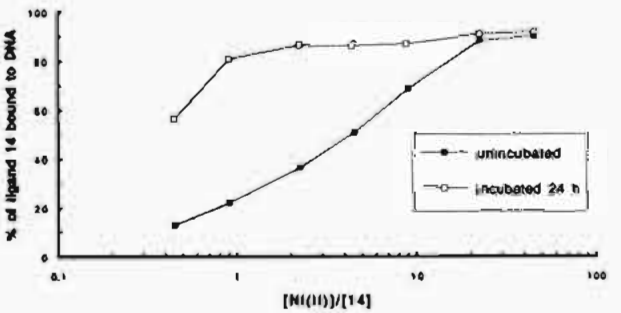

Figure 17. Effect of increasing [$MgCl_2$] on binding of **14** to DNA in the presence of $Ni(NO_3)_2$. Concentrations were as follows: [DNA(P)], 1.2 mM; [**14**], 50 μM; $Ni(NO_3)_2$, 100 μM. Order of addition to the ultrafiltration device was DNA, $MgCl_2$, and **14**–$Ni(NO_3)_2$ mixture.

when the concentration of NaCl is 500 times that of the **14**–Ni(II) complex.

Figure 17 shows the same study conducted with the divalent cation Mg^{2+} (as $MgCl_2$). The Mg^{2+} affects the binding of the metal/ligand complex to DNA at a concentration 100 times that of Ni(II). Nearly complete loss of binding is observed at concentrations of Mg^{2+} 3000 times that of Ni(II).

A similar study was performed with spermine, a tetracation at pH 8 that is known to bind strongly to DNA.[25] Spermine also affected the binding of the metal–ligand complex to DNA.

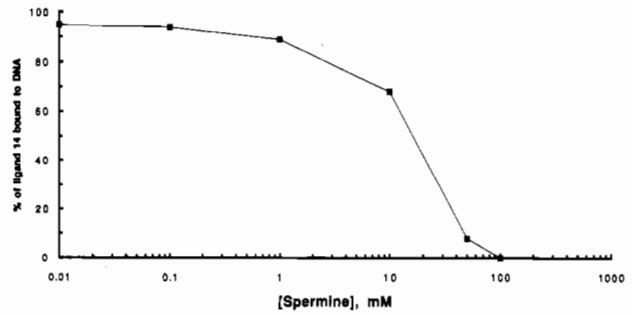

Figure 18. Effect of increasing [spermine] on binding of **14** to DNA in the presence of $Ni(NO_3)_2$. Concentrations were as follows: [DNA(P)], 1.2 mM; [**14**], 50 μM; [$Ni(NO_3)_2$], 100 μM. Order of addition to the ultrafiltration device was DNA, spermine, and **14**–$Ni(NO_3)_2$ mixture.

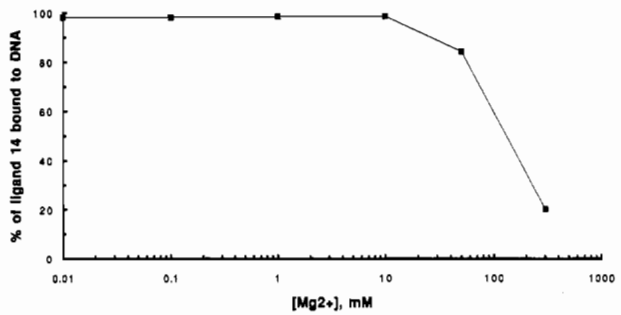

Figure 19. Effect of varying $Ni(NO_3)_2$ concentration and preincubation of metal and ligand on binding of **14** to DNA. In all experiments [DNA(P)] was 600 μM and [**14**] was 50 μM. In the unincubated case, $Ni(NO_3)_2$ was mixed with DNA before addition of **14**, while in the incubated case, $Ni(NO_3)_2$ and **14** were premixed and then added to the DNA solution. Graph shows the percent of the total ligand bound to DNA after ultrafiltration.

Binding first became disrupted when the spermine concentration was 10 times that of Ni(II), and was completely disrupted at levels 500 times that of Ni(II). Even at a spermine concentration of 10 mM, a factor of 100 greater than Ni(II), and 8 times that of DNA phosphates, 70% of the ligand was still retained on the DNA side of the ultrafiltration membrane. This suggests that the binding of the metal complex is not solely the result of electrostatic interactions between the negatively charged DNA phosphates and the tetracationic metal complex, since binding of the metal–ligand complex is not dramatically affected by comparable spermine concentrations. If the spermine were competing with the metal–ligand complex only as a tetracation, it would be expected that the binding would be completely disrupted at this concentration of spermine. Figure 19 shows the effect of variations in the nickel ion concentration on the binding of ligand **14** to DNA. It also demonstrates the importance of preassociation of the ligand with the metal before complexation to the DNA. For the experiments in which the metal and ligand were allowed to preassociate, the percent of the total ligand bound to DNA reached its maximum at a Ni:ligand ratio of 2:1, as would be predicted if each bis(imidazole) binding site is complexed to one Ni(II). However, at a Ni:ligand ratio of 1:1, approximately 80% of the ligand was complexed to DNA. This is significantly higher than expected if a 2:1 Ni–ligand complex is the sole DNA binding agent. As the 2:2 Ni–ligand complexes also have coordination sites available for bidentate DNA binding, it appears that both the 2:2 and 2:1 complexes are involved in DNA coordination. The level of binding for unincubated cases was significantly lower than for those which were allowed to incubate. This suggests that the metal–ligand complexes must be formed prior to the DNA binding event. In the absence of precoordination to the ligand, the metal may directly coordinate to the DNA.[1]

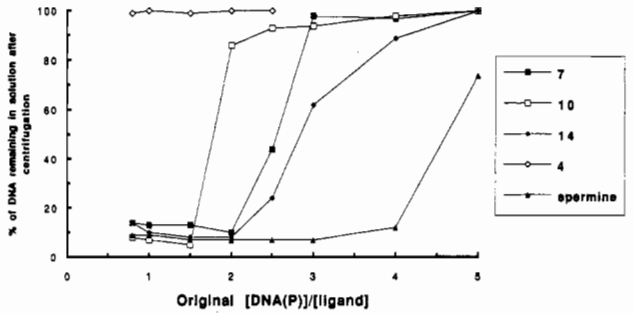

Figure 20. Precipitation of DNA by various ligand–metal complexes and by spermine. In all cases, [DNA(P)] was varied while [ligand] was held constant (0.10 mM for **7**, **10**, **14**, and spermine; 0.20 mM for **4**). $Ni(NO_3)_2$ was present at a concentration of 0.20 mM in all experiments except for that of spermine, where it was omitted. Graph shows percent of DNA remaining in solution after samples were centirifuged 1 h in a microcentrifuge.

Precipitation Studies. It is well known that a variety of cations cause precipitation of DNA.[26] In particular, spermine, which is a tetracation at pH 8, is extremely effective at causing DNA to precipitate from aqueous solution.[26] With this in mind, a series of experiments were performed to determine if the polyimidazole systems **4**, **7**, **10**, **14**, and **15** would cause DNA to precipitate in the presence of Ni(II). All ligands were tested with sonicated calf thymus DNA. A series of experiments were conducted with each ligand, wherein aliquots of a Ni(II)–ligand solution were added to various concentrations of DNA. Concentrations were chosen to give ratios of DNA phosphates to ligand ratios in a range from 0.2 to 5. Figure 20 shows the results of these studies.

The percent of DNA remaining in solution after centrifugation is plotted against the ratio of DNA phosphates:ligand added. In all cases, one equivalent of Ni(II) was present for every two imidazole groups. Spermine was quite effective at precipitating DNA with complete precipitation being achieved at levels of approximately 1 equivt of spermine for every four DNA phosphates. This is not surprising since, as a tetracation, this ratio would give complete neutralization of the negatively charged DNA phosphates. The bis(methylimidazole) **4** in the presence of Ni(II) caused no precipitation of the DNA. This was expected since in our other studies, this ligand had not been found to bind strongly to the DNA. The other tetrakis(methylimidazole) ligands **7**, **10**, **14**, and **15** in the presence of 2 equiv of Ni(II), caused complete precipitation of the DNA at ratios of DNA phosphates to ligand in the range of 1.5:1 to 2:1. Control experiments with just ligands or just $Ni(NO_3)_2$ resulted in no appreciable amounts of precipitation of DNA.

Discussion

We have prepared a series of methylimidazole-containing ligands which, in the presence of Ni(II) or Zn(II) ions, retard the migration of DNA on agarose gel electrophoresis. Simple ion pairing between the positively charged transition metal ions and the negatively charged phosphates was thought not to be involved, because the electrophoretic mobility of the DNA was affected to varying degrees by ligands that differ only in the stereochemistry of the tether between the two metal binding sites. Tetrakis(methylimidazole) ligands **7**–**11**, which contain flexible alkyl spacers, did not significantly affect DNA mobility, while ligand **5**, containing the rigid aromatic spacer, and ligands **14**–**17**, containing rigid octahydropentalene spacers, caused retardation of DNA migration in the presence of 2 equiv of Ni(II) or Zn(II) cations. Furthermore, each ligand that influenced DNA mobility did so to a different degree. For example, ligand **14** slowed DNA

(25) (a) Bloomfield, V. A.; Wilson, R. A. In *Polyamines in Biology and Medicine*; Morris, D. R., Marton, L. J., Eds.; Marcel Dekker, Inc.: New York, 1981; Chapter 10. (b) Feuerstein, B. G.; Williams, L. D.; Basu, H. S.; Marton, L. J. *J. Cell. Biochem.* **1991**, *46*, 37–47.

(26) Margerum, D. W.; Cayley, G. R.; Weatherburn, D. C.; Pagenkopf, G. K. In *Coordination Chemistry*; Martell, A. E., Ed.; ACS Monograph 174; American Chemical Society: Washington, DC, 1978; Vol. 2, pp 1–221.

migration to a much greater extent than did ligand **15** (in the presence of Ni(II) or Zn(II)). Control experiments were performed wherein DNA was run on agarose gels in the presence of ligand without metal and in the presence of metal without ligand. A dimetal complex is implicated, since mononuclear complexes of diimidazole ligand **4** showed no inhibitory effect on gel mobility. In both cases no change in DNA mobility was observed, suggesting that a ligand–metal complex is responsible for the observed inhibition of gel mobility.

In order to determine the fate of the ligands in the gel electrophoresis experiments, and study the DNA/ligand–metal interactions further, several of the ligands were labeled with tritium. The radiolabeling procedure entailed metallation of the imidazoles with *t*-butyllithium, followed by quenching with tritiated water. Agarose gels run with radiolabeled analogues of ligands **10**, **14**, and **15** demonstrated that the ligands do not remain bound to the DNA during electrophoresis. Table XIV (supplementary material) and Figure 15, show that in gel slices which contained DNA (lanes 2–4, slices labeled C–E) no counts were found above background levels. Evidently the ligand–metal complexes dissociate from the DNA as electrophoresis proceeds. Gel slices located closer to the origin (slices A and B) contained the radiolabeled ligand, suggesting that the DNA had brought the ligands into the gel but that the ligands had dissociated from the DNA during the course of the electrophoresis experiment.

DNA with bound metal–ligand complex will migrate more slowly through the gel due to charge neutralization by the transition metal cations. In the extreme case, when all the charge of the DNA is neutralized, the DNA will not move at all. As the ligand–metal complexes dissociate from the DNA, the rate of DNA migration will increase to a maximum when all of the ligand–metal complex has been removed. The released cationic metal complex should migrate back rapidly toward the well. The period of time between the start of the electrophoresis and the point at which all of the ligand–metal complex has dissociated from the DNA will determine the extent to which slowing and streaking of the DNA are observed. Evidently, complexes containing ligands with flexible alkyl spacers (**7–11**) dissociate from the DNA much more rapidly than those with rigid spacers (**5**, **14–17**).

There are several ways in which the ligand–metal complexes might interact with the DNA framework. Electrostatic interaction of the positively charged transition metals with the negatively charged phosphate groups of the DNA backbone,[1] coordination of the transition metal ions with nitrogen bases of the DNA, analogous to the manner in which cisplatin binds to DNA[4], and a combination of the two, are several of the possibilities that one might consider. NMR studies of the zinc complexes and X-ray crystal data for the nickel complexes both show that there are indeed vacant coordination sites on the metals, which could in turn coordinate to basic sites on the DNA. NMR studies of ligands **4**, **14**, and **15** in the presence of increasing amounts of $Zn(NO_3)_2$ (Figures 7–9) reveal that, in solution, a complex equilibrium exists involving several different ligand–metal species. One of the major species involving tetra(methylimidazole) ligands **14** and **15** is the 2:1 Zn–ligand complex, in which the metal ions have additional coordination sites available for DNA coordination. This could be viewed as a tetracationic DNA binding agent.

X-ray crystal structures of nickel complexes were solved for complexes **18–20**, which had been prepared by adding 2 equiv of Ni(II) to 1 equiv of tetrakis(methylimidazole) ligands **15**, **10**, and **7**, respectively. These crystallizable complexes all had Ni:ligand ratios of 2:2, in contrast to the zinc complexes, in which the major solution species had a Zn:ligand ratio of 2:1. However, in the case of zinc, a complex equilibrium exists in solution. It is likely that the same type of equilibrium exists in solution in the case of nickel and that a significant amount of the 2:1 Ni–ligand species is present. The isolated crystals probably reflect the favorable packing of the 2:2 complex. In the 2:2 Ni–ligand complexes, such as **18–20**, each octahedral nickel ion has only four of six sites filled by methylimidazole groups from the ligands. The remaining sites, which in the isolated complexes are filled by labile water, nitrate, or bridging chloride ligands, are also candidates for ligand exchange and DNA coordination.

These crystal structures also confirm the expected lack of cooperativity between the metals in compounds with flexible methylene spacers, and the close proximity dictated by the rigid octahydropentalene spacer in **15**. Furthermore the conformation of **15** in the Ni(II) complex closely resembles that predicted for the free ligand. Each cyclopentane ring has an envelope conformation with the envelope flaps at C_2 and C_5 folded away from the methyl substituents at C_{3a} and C_{6a}. Molecular models and molecular mechanics calculations suggest that diastereomer **14**, for which a crystal structure is not available, will prefer a conformation with C_2 and C_5 folded toward the angular methyl substituents in order to avoid transannular interactions between the bulky substituents at C_2 and C_5. In such a conformation, the orientation of the imidazole to form a 2:2 complex with a bridging chloride does not appear to be as favorable as with **15**. Molecular models also suggest that both **14** and **15** are capable of forming 2:2 complexes analogous to **19** and **20** but with considerably shorter metal–metal distances and orientations.

Since polycations, such as spermine or spermidine, are known to interact with DNA and cause its precipitation, the precipitation of DNA by ligands **4**, **7**, **10**, and **14** in the presence of Ni(II) was studied to determine if these systems would have a similar effect. As shown in Figure 20, the tetra(methylimidazole) ligands **7**, **10**, and **14** were indeed found to cause precipitation of DNA in the presence of 2 equiv of $Ni(NO_3)_2$. Neither Ni(II) alone nor ligand alone caused precipitation. Bidentate ligand **4**, which can only form a mononuclear complex, did not cause precipitation in the presence of Ni(II) cations. DNA precipitation was observed to occur at a DNA phosphate:ligand ratio of 1.5:1 (for **10**) to 2:1 (for **7** and **14**). This differs from spermine, a tetracation at pH = 8, which induces DNA precipitation at a DNA phosphate:ligand ratio of 4:1.[25] If precipitation occurs near the point at which charge neutralization occurs, this suggests that with Ni(II) the 2:2 ligand–metal complex may be the dominant DNA binding agent. This hypothesis is supported by studies in which the amount of ligand bound to DNA at various concentrations of Ni(II) was investigated (Figure 19). At a ratio of metal to ligand of 2:2, approximately 80% of the ligand was bound to the DNA whereas at a ratio of 2:1 or higher approximately 87% of the ligand was bound. The 2:2 ligand–metal complex would neutralize the charge of the phosphates at a DNAP:ligand ratio of 2:1, whereas with the 2:1 ligand–metal complex, charge neutralization would occur at a DNAP:ligand ratio of 4:1. In the 2:2 complex, each metal has two coordination sites available for DNA coordination. Because of the dynamic nature of the coordination process it is likely that both the 2:1 and 2:2 complexes are involved in DNA coordination.

The ultrafiltration studies, presented in Table XVI, demonstrate that, in the presence of Ni(II) or Zn(II), tetrakis(methylimidazole) binucleating ligands **7**, **10**, **14**, and **15** bind to DNA, while the bis(methylimidazole) ligand **4** does not. These results were initially somewhat surprising since there was little difference in the ultrafiltration binding behavior of the various tetrakis(methylimidazole) ligands. In the gel electrophoresis studies, ligands with flexible alkyl spacers had no effect on DNA mobility while ligands that contained more rigid spacers had a profound effect.

Conclusions

Although the binuclear metal complexes were not significantly more active than mononuclear analogues for the catalytic hydrolysis of phosphate diesters, they were significantly better

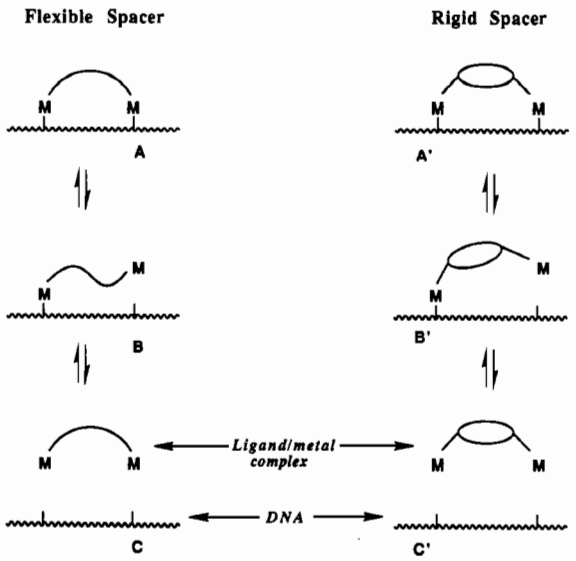

Figure 21. Analysis of DNA binding by binuclear transition metal complexes. Complex containing a flexible spacer is depicted at left, and one containing a rigid spacer is shown on the right. Key: top, both metals bound, center, one metal bound and one free, bottom, both metals free.

DNA binding agents. Even the normally labile metal ions Zn(II) and Ni(II) formed complexes that bound strongly enough to DNA to affect its mobility in gel electrophoresis experiments. Such changes in gel mobility are well known when kinetically nonlabile metal ions, such as Pt(II) complexes, bind to DNA.

In order to better understand the behavior of these ligand–metal complexes in the presence of DNA, one must consider the physical phenomena involved in both the gel electrophoresis and ultrafiltration experiments. In the ultrafiltration experiments, an equilibrium between the bound and unbound states is established. Rapid filtration permits separation and quantitation of the bound and unbound species. Thus, one is allowed to view the thermodynamic equilibrium of the binding process. Gel electrophoresis, however, is a dynamic process wherein the kinetics of the dissociation event play a critical role. In the electric field, the negatively charged DNA migrates through the gel toward the positive electrode while the positively charged ligand–metal complex, when not coordinated to the DNA framework, will migrate in the direction of the negative electrode. The inhibition of mobility in the gel electrophoresis experiments is thus influenced by the kinetics at which the metal complex dissociates from DNA.

With binucleating ligands having flexible alkyl spacers, DNA gel mobility is not affected. On electrophoresis, these complexes must dissociate from DNA much faster than do complexes containing ligands with rigid spacers. Since the manner in which each metal coordinates to DNA is likely to be similar, the differences in binding behavior appear to be due to variations in the nature of the spacer in different ligand:metal complexes.

A simplistic view of the dissociation process is presented in Figure 21. In **A** and **A'**, the metal–ligand complexes have both metals bound to the DNA. In the first step of the dissociation process, one of the metals dissociates from the DNA to give intermediates **B** and **B'**. In the second step, the second metal dissociates from the DNA to give the free complex, as shown in **C** and **C'**. In the DNA complexes of ligands with rigid spacers, it is difficult for the first metal dissociation step to occur because the rigid spacer unit lacks the conformational flexibility necessary for the first dissociating metal to migrate away from the DNA framework. However, with ligands having flexible spacers, after the first metal dissociates, the conformational freedom of the tether allows the metal to migrate away from the DNA binding site. Once the first metal dissociates and migrates away from the DNA, the second metal will readily dissociate. This situation resembles the well-known kinetics of metal ion release from chelating ligands wherein increased conformational flexibility increases the rate of metal ion dissociation and reduces the stability of the complex.[26] This resembles a chelate effect with DNA as the binding site and the binuclear metal complex as the ligand.

These studies underscore the problems in quantifying DNA–metal complex binding, particularly in cases where the metals retain open coordination sites for interaction with DNA. In the gel mobility studies, the kinetics of metal complex release appear to play an important role, while ultrafiltration membrane measurements of binding are less susceptible to such effects. Binuclear metal complexes show a markedly enhanced binding affinity for DNA over corresponding mononuclear complexes, as evidenced by gel mobility, ultrafiltration, and precipitation experiments. On the basis of the ultracentrifugation data presented in Table XVI, it appears that the enhancement of binding ability is in the general area of 10^3–10^5. Competition experiments show that the bimetallic complexes bind DNA much more effectively than simple polycations, such as spermine. This suggests that, in addition to an electrostatic attraction, the metals ligate DNA at either the phosphate backbone oxygens or nitrogen base sites.

As demonstrated in the gel electrophoresis studies, the conformational flexibility of the tether between two chelated metals can dramatically effect the interaction of these complexes with DNA. Though not directly involved in coordination to the DNA, the geometry and rotational freedom of the tether can potentially have a dramatic impact on the DNA binding affinity of polyfunctional DNA binding agents. Such effects should be taken into account when designing new polyfunctional DNA binding agents.

Acknowledgment. We are grateful for partial support from the National Institutes of Health (Grant GM 39972 to D.F.H.), the American Cancer Society (Junior Faculty Research Award to D.F.H.) and the National Science Foundation (Grant CHE-88015958 to W.C.T.). The 500–MHz NMR spectrometer was purchased with assistance from the NIH (RR04733) and the NSF (CHE 8814866). Mass spectra were obtained at the University of California at Riverside Mass Spectrometry Facility. Fellowship support to E.K. from Eli Lilly and Syntex is gratefully acknowledged.

Supplementary Material Available: Tables II–VII and XI–XIV, giving atomic coordinates and equivalent isotropic displacement coefficients and bond distances and bond angles for **18–20** and deuterium labeling studies with **15**, **4**, **10**, and **7**, respectively (19 pages). Ordering information is given on any current masthead page.